Stem Cell Reports
Article
ISSCR
OPEN ACCESS

Generation of functionally competent hepatic stellate cells from human stem cells to model liver fibrosis *in vitro*

Xinyuan Lai,[1,6] Chuanyun Li,[2,6] Chengang Xiang,[3,5] Zihang Pan,[1] Kai Zhang,[1] Lei Wang,[1] Bingqing Xie,[3] Junning Cao,[4] Jihang Shi,[4] Juan Deng,[1] Shichun Lu,[4] Hongkui Deng,[3] Hui Zhuang,[1] Tong Li,[1,*] Yan Shi,[3,*] and Kuanhui Xiang[1,*]

[1]Department of Microbiology and Infectious Disease Center, School of Basic Medical Sciences, Peking University Health Science Center, Beijing 100191, China
[2]Center of Liver Transplantation, Beijing Youan Hospital, Capital Medical University, Beijing 100069, China
[3]School of Basic Medical Sciences, State Key Laboratory of Natural and Biomimetic Drugs, Peking University Health Science Center, Beijing 100191, China
[4]Department of Hepatobiliary Surgery, First Medical Center of Chinese PLA General Hospital, Beijing 100039, China
[5]Renal Division, Peking University First Hospital, Beijing 102218, China
[6]These authors contributed equally
*Correspondence: toglii97@bjmu.edu.cn (T.L.), shiyan@bjmu.edu.cn (Y.S.), kxiang@bjmu.edu.cn (K.X.)
https://doi.org/10.1016/j.stemcr.2022.09.010

SUMMARY

The detailed understanding of fibrogenesis has been hampered by a lack of important functional quiescence characteristics and an *in vitro* model to recapitulate hepatic stellate cell (HSC) activation. In our study, we establish robust endoderm- and mesoderm-sourced quiescent-like induced HSCs (iHSCs) derived from human pluripotent stem cells. Notably, iHSCs present features of mature HSCs, including accumulation of vitamin A in the lipid droplets and maintained quiescent features. In addition, iHSCs display a fibrogenic response and secrete collagen I in response to hepatoxicity caused by thioacetamide, acetaminophen, and hepatitis B and C virus infection. Antiviral therapy attenuated virally induced iHSC activation. Interestingly, endoderm- and mesoderm-derived iHSCs showed similar iHSC phenotypes. Therefore, we provide a novel and robust method to efficiently generate functional iHSCs from hESC and iPSC differentiation, which could be used as a model for hepatocyte toxicity prediction, anti-liver-fibrosis drug screening, and viral hepatitis-induced liver fibrosis.

INTRODUCTION

Liver fibrosis is a characteristic of disease progression in chronic inflammatory disease caused by viral hepatitis and hepatic toxicity, contributes to disfunction of the liver, and represents the major risk factor in development of hepatocellular carcinoma (HCC) (Roehlen et al., 2020). Liver cirrhosis developing from liver fibrosis is currently the 11th most common cause of death in the world (Asrani et al., 2019).

The activation of hepatic stellate cells (HSCs) might be one of the most important pathogenic mechanisms of liver fibrosis; they produce collagen and are also involved in angiogenesis during the early stage of the fibrosis process. The HSCs are one of the important non-parenchymal components of the space of Disse, the lining between hepatocytes and endothelial sinusoidal cells with multiple functions in the liver. Normally, HSCs accumulate vitamin A in lipid droplets in the healthy liver and express mature HSC markers like glial fibrillary acidic protein (GFAP), desmin, activated leukocyte cell adhesion molecule (ALCAM), protocadherin 7 (PCDH7), neural cell adhesion molecule (NCAM), and platelet-derived growth factor receptor (PDGFR) α and PDGFRβ (Friedman, 2008). In response to liver injury, activated HSCs (aHSCs) are transformed into myofibroblasts (Friedman, 2008). The aHSCs are characterized by decreased vitamin A storage and peroxisome proliferator-activated receptor γ (PPARγ) expression, but increased proliferation and high contractility, with expression of activation-related proteins, such as α-smooth muscle actin (α-SMA), nestin, and vimentin; secretion of abundant extracellular matrix proteins (fibronectin and collagens) (Shang et al., 2018); and possibly expressing stellate cell activation-associated protein (STAP) (Kawada et al., 2001).

However, a detailed understanding of HSC activation has been hampered by the scarcity of efficient *in vitro* cell models. Primary HSCs (pHSCs) are the "gold standard" model for the study of liver fibrosis. However, pHSCs easily lose their quiescent features and are activated during the cell isolation and culture process into collagen type I-producing myofibroblasts (aHSCs), which limits their study to the mechanism of HSC activation. Moreover, pHSCs are very difficult to isolate from liver donors. The pHSCs are also heterogeneous among different donors, and contain considerable variation because of the diverse cell isolation processes in different laboratories (Gutierrez-Ruiz and Gomez-Quiroz, 2007; Mederacke et al., 2015). Because of the lack of cell source, the knowledge of important functional characteristics and the activated phenotype of pHSCs is quite limited, which restricts the application of pHSCs. Immortalized HSC lines have been

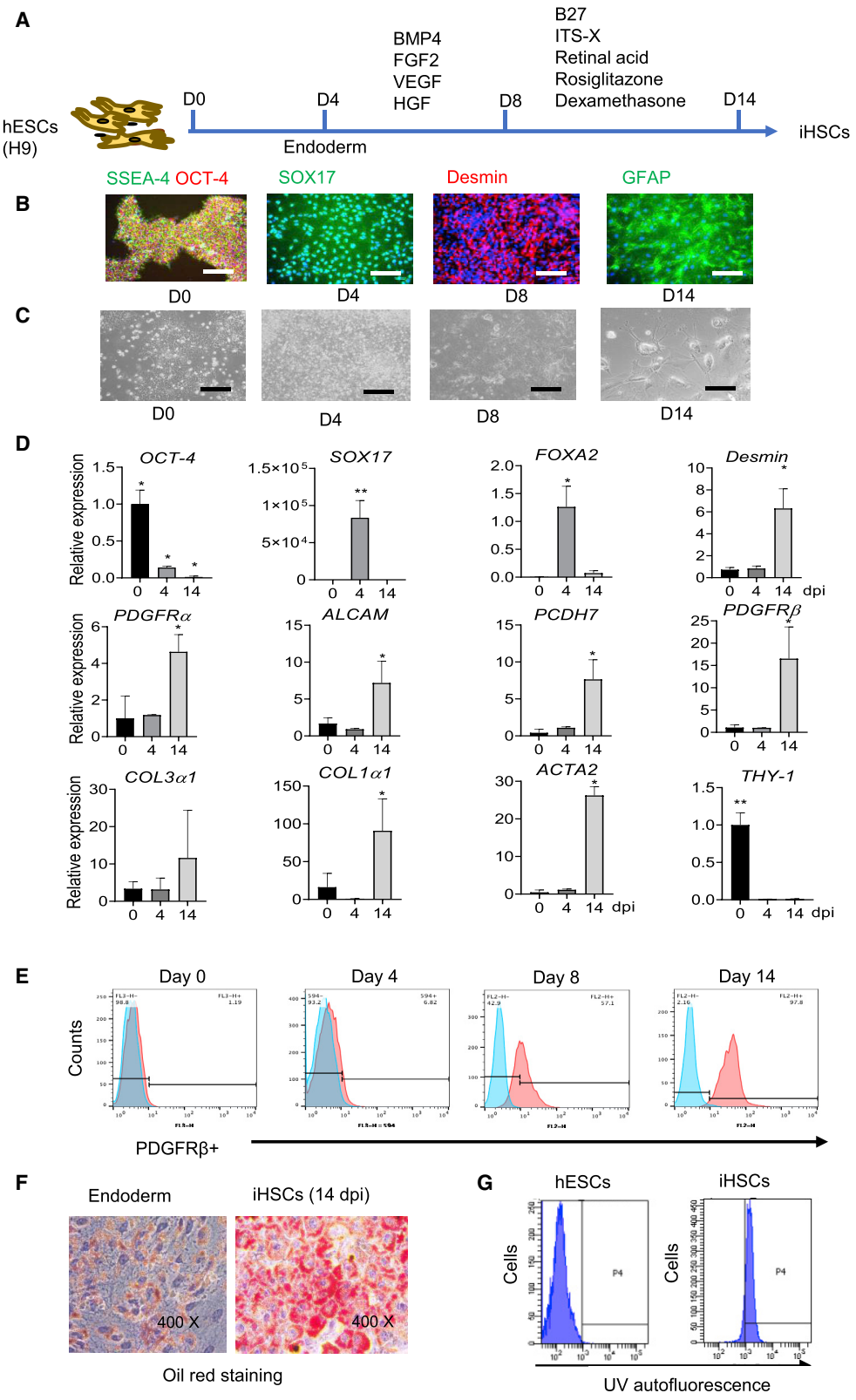

(legend on next page)

established and are used in a wide range of research. These immortalized cell lines provide unlimited HSCs (Xu et al., 2005). The immortalized cell models, such as LX-2, generated by transformation with SV40 T antigen, are still used to model fibrogenic gene expression in HSCs induced by hepatitis virus infection (Akil et al., 2019). However, it is not easy to maintain the quiescent features of LX-2 cells *in vitro*, which is a deviation from the natural pHSCs (Ajat et al., 2017; Perea et al., 2015).

There are, however, alternative sources of HSCs from stem cell differentiation, such as human embryonic stem cells (hESCs) and human induced pluripotent stem cells (iPSCs). Unlike pHSCs, these cells potentially provide a renewable HSC source because of their unlimited expansion and differentiation capacity, and they can differentiate into parenchymal and non-parenchymal liver cells (Iacob et al., 2011; Koui et al., 2017). They can also be genetically manipulated to make personalized models for drug screening. Coll et al. reported that a combination of fibroblast growth factors (FGF1 + FGF3) could induce PSCs to become HSC-like cells (induced HSCs [iHSCs]), while FGF2 lacked this function (Coll et al., 2018). Another study showed that only bone morphogenetic protein 4 (BMP4) and FGF2 could induce mesoderm into iHSCs, which is controversial compared with the Coll et al. report (Miyoshi et al., 2019). However, both of these strategies still suffer from several shortcomings, including the lack of quiescent character and limited function of the target cells.

Here, we describe a new fibrogenesis model based on direct differentiation of hESCs and iPSCs into both endoderm- and mesoderm-derived iHSCs, which possess the features of quiescent HSCs (qHSCs). The iHSCs highly resemble freshly isolated qHSCs in cell identity and functionality, which are important for studying the mechanism of HSC activation during the early stage of liver fibrosis. Importantly, iHSCs support a fibrogenic response to hepatoxicity caused by thioacetamide and acetaminophen and viral infection by hepatitis B virus (HBV) and hepatitis C virus (HCV), which suggests a broad application potential for hepatotoxic and viral hepatitis-related liver fibrosis modeling and drug discovery.

RESULTS

Generation of the endoderm-derived iHSCs from human embryonic stem cells

Different protocols have been described for differentiating hESCs and iPSCs into iHSCs (Coll et al., 2018; Miyoshi et al., 2019). The main challenges are to obtain qHSCs that exhibit a feature of mature HSCs and can be activated by stimulators such as TGF-β. Moreover, only mesoderm-derived iHSCs were differentiated from ESCs. However, differentiation derived from other blastoderms such as endoderm or ectoderm has rarely been reported. Therefore, we focused on establishing and optimizing a differentiation protocol from endoderm to iHSCs. From the analysis of vascular endothelial growth factor (VEGF) expression in HSCs and the potential roles of hepatic, hematopoietic, and neuronal differentiation and regeneration based on previous studies (Wang et al., 2012; Jin et al., 2018; Theis and Theiss, 2018), we combined BMP4 with FGF2 and VEGF to induce hESC (H9)-derived iHSC differentiation. Moreover, PPARγ has been discovered as a new transcription factor for regulating the phenotype of HSCs. After modification by addition of the PPARγ agonist rosiglitazone (Liu et al., 2020b), the differentiation of iHSCs showed high PDGFRβ expression and lower α-SMA and collagen I expression (data not shown), indicating its importance in mature iHSC differentiation.

Finally, we established and optimized our methods to differentiate stem cells more efficiently and quiescently into endoderm-derived mature HSCs capable of reflecting phenotypes from qHSCs to aHSCs. Thus, mature iHSCs were obtained from hESCs or iPSCs through a three-step

Figure 1. Distinct HSC marker expression in iHSCs during differentiation

(A) Schematic representation of the differentiation process from day 0 to day 14. The related marker expression is shown in (B) to (G).

(B) Representative images of hESC-, endoderm-, and iHSC-related markers during the different stages of iHSC differentiation according to the protocol shown in (A). Scale bars, 100 μm.

(C) Representative images of cell morphology on days 0, 4, 8, and 14 of differentiation. Scale bars, 100 μm.

(D) qRT-PCR analyses of the gene expression kinetics of an hESC marker (*OCT-4*), endoderm markers (*SOX17* and *FOXA2*), HSC markers (*Desmin*, *ALCAM*, *PCDH7*, *PDGFRα*, and *PDGFRβ*), activated HSC markers (*Col1α1*, *Col3α1*, and *ACTA2*) and a fibroblast marker (*THY-1*) during differentiation. Data are shown as the mean ± SEM from three independent experiments; n = 3 in each group.

(E) Representative histograms of flow cytometric analysis of PDGFRβ expression during differentiation. Positive gates were defined based on the isotype control. See also Figures S1A and S1B.

(F) Oil red analysis of lipid droplets in the iHSCs. See also Figure S1C.

(G) Flow cytometry analysis of autofluorescence of intracellular vitamin A droplets in iHSCs (right). Human embryonic stem cells (hESCs) are used as a control (left). See also Figure S1D. Data are shown as the mean ± SEM from three independent experiments. Student's t test was used. *$p < 0.05$; **$p < 0.01$.

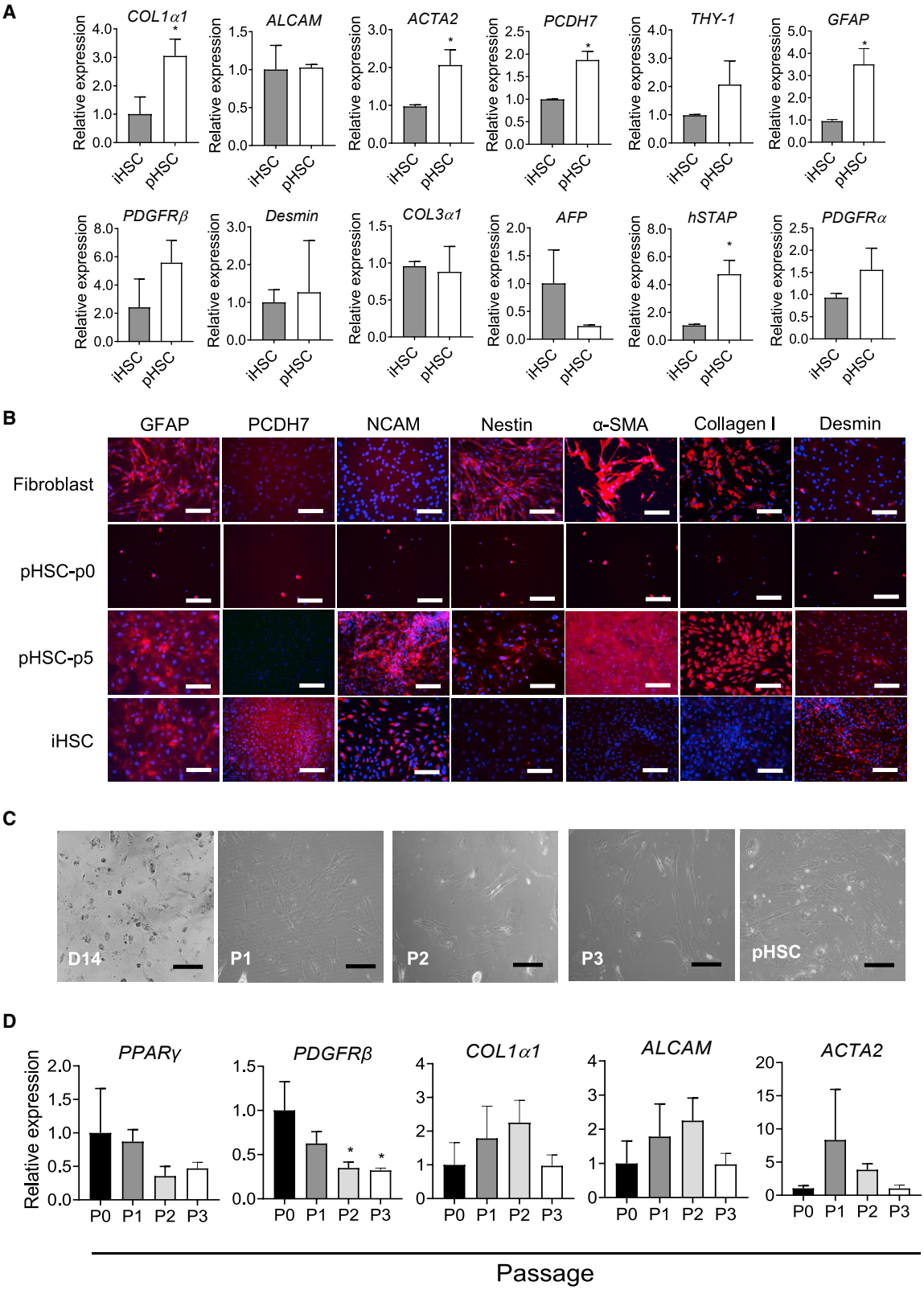

(legend on next page)

differentiation protocol (Figure 1A). Undifferentiated hESCs (H9) were incubated with STEMdiff definitive endoderm differentiation medium for 4 days to induce endoderm. Following this step, the cells were incubated with BMP4, FGF2, VEGF, and hepatocyte growth factor (HGF) for another 4 days. Then, the continued differentiation to iHSCs was performed by incubation of the cells with retinoic acid, dexamethasone, and rosiglitazone from day 8 to day 14. Figure 1B shows the immunofluorescent staining of markers expressed at specific stages during the cell differentiation. The hESCs expressing octamer-binding transcription factor 4 (OCT-4) and stage-specific embryonic antigen 4 (SSEA-4) were differentiated into endoderm with SOX17 expression. Then, the endoderm was differentiated into iHSCs with desmin and GFAP expression, which is associated with HSCs. Representative pictures of cell morphology during the differentiation stages are displayed in Figure 1C.

Using this protocol, we detected the markers expressed in embryonic development and mature HSCs during differentiation. As shown in Figure 1D, the transcripts of HSC-related markers, such as *desmin*, *PDGFRα*, *ALCAM*, *PCDH7*, and *PDGFRβ* were significantly increased toward the end of the differentiation at 14 days post induction (dpi), while the fibroblast-related marker *THY-1* was rarely detected. HSC activation-related transcript markers collagen type 1α 1 chain (*COL1α1*), collagen type 3α 1chain (*COL3α1*), and α2-SMA (*ACTA2*) in iHSCs were expressed relatively higher than in the hESCs and endoderm. However, their protein levels detected by flow cytometry were very low, indicating that collagen I and α-SMA expression of iHSCs was very low by our protocol (Figure S1A).

To further evaluate the generation of HSCs from hESCs, we detected PDGFRβ expression, which was reported as one of the best membrane markers of HSCs, by flow cytometry. As shown in Figures 1E and S1B, the percentage of PDGFRβ$^+$ cells increased during the differentiation, from 1% in hESCs to more than 90% in iHSCs at 14 dpi. In addition, we further assessed the vitamin A storage in the lipid droplets in iHSCs. First, oil red staining showed that all of the cells were rich with lipid droplets, while endoderm showed poor lipid droplet content (Figures 1F and S1C). Then, we measured vitamin A by rapid bleaching with UV light and flow cytometry. As shown in Figures 1G and S1D, hESCs and endoderm showed no vitamin A$^+$ cells, while more than 90% of iHSCs and pHSCs were positive with vitamin A. These data suggest that iHSC differentiation via this protocol obtained the stellate cell identity.

Characterization of iHSCs compared with pHSCs

To better evaluate the characteristics of iHSCs in this protocol, we compared the differentiated iHSCs on day 14 with pHSCs (passage 3). As shown in Figure 2A, iHSCs and pHSCs expressed similar levels of *ALCAM*, *PDGFRβ*, *desmin*, and *PDGFRα*. By contrast, pHSCs expressed relatively higher *PCDH7* and *GFAP* levels than iHSCs, indicating the difference between iHSCs and pHSCs. Notably, pHSCs could be easily activated during the present culture conditions. Thus, markers of stellate cells, *hSTAP*, *COL1α1*, and *ACTA2*, were expressed lower in iHSCs than in pHSCs. In addition, we further compared HSC markers among fibroblasts, pHSCs passage 0 (p0), pHSCs p5, and iHSCs by immunofluorescent staining. Passage 0 had a low number of cells due to no cell proliferation. As shown in Figure 2B, at the end of the differentiation, iHSCs expressed specific HSC markers, such as GFAP, PCDH7, NCAM, and desmin, while they expressed nearly no nestin, α-SMA, or collagen I (markers expressed in fibroblasts and aHSCs). The activated markers (e.g., nestin, α-SMA, and collagen I) were positive in both pHSCs p0 and pHSCs p5, indicating that pHSC activation might happen in the liver or during isolation and culture. Fibroblasts expressed only GFAP, nestin, α-SMA, and collagen I, which showed similar features compared with aHSCs.

To evaluate the effect of subculturing iHSCs on themselves, we assessed the expression of iHSC markers at three passages. Representative pictures of cell morphology during the different passages are displayed in Figure 2C. As shown in Figure 2D, most of the iHSC markers showed similar expression levels during the passages, except for *PDGFRβ*, which showed significantly decreased expression during the subculture. These data suggest that iHSCs can maintain the expression of key HSC markers during passage.

Transcriptome analysis of iHSCs

To further evaluate the overall characteristics of iHSCs, we did RNA sequencing to generate transcriptomic profiles of endoderm-derived iHSCs (iHSCs_end), mesoderm-derived

Figure 2. The HSC marker expression in iHSCs compared with pHSCs

(A) qRT-PCR analysis of gene expression of HSC markers (*ALCAM*, *PCDH7*, *GFAP*, *PDGFRβ*, *Desmin*, *hSTAP*, and *PDGFRα*), a fibroblast marker (*THY-1*), activated HSC markers (*COL1α1*, *COL3α1*, and *ACTA2*), and a hepatic marker (*AFP*); n = 3 in each group.

(B) Representative images of the markers GFAP, PCDH7, NCAM, nestin, α-SMA, collagen I, and desmin in iHSCs, pHSCs (p0 and p5), and fibroblast cells. Scale bars, 100 μm.

(C) Representative images of the iHSC morphology at different passages of iHSCs and pHSCs. Scale bars, 100 μm.

(D) qRT-PCR analysis of gene expression in iHSCs at different passages. Data are shown as the mean ± SEM from three independent experiments; n = 3 in each group. Student's t test was used. *p < 0.05.

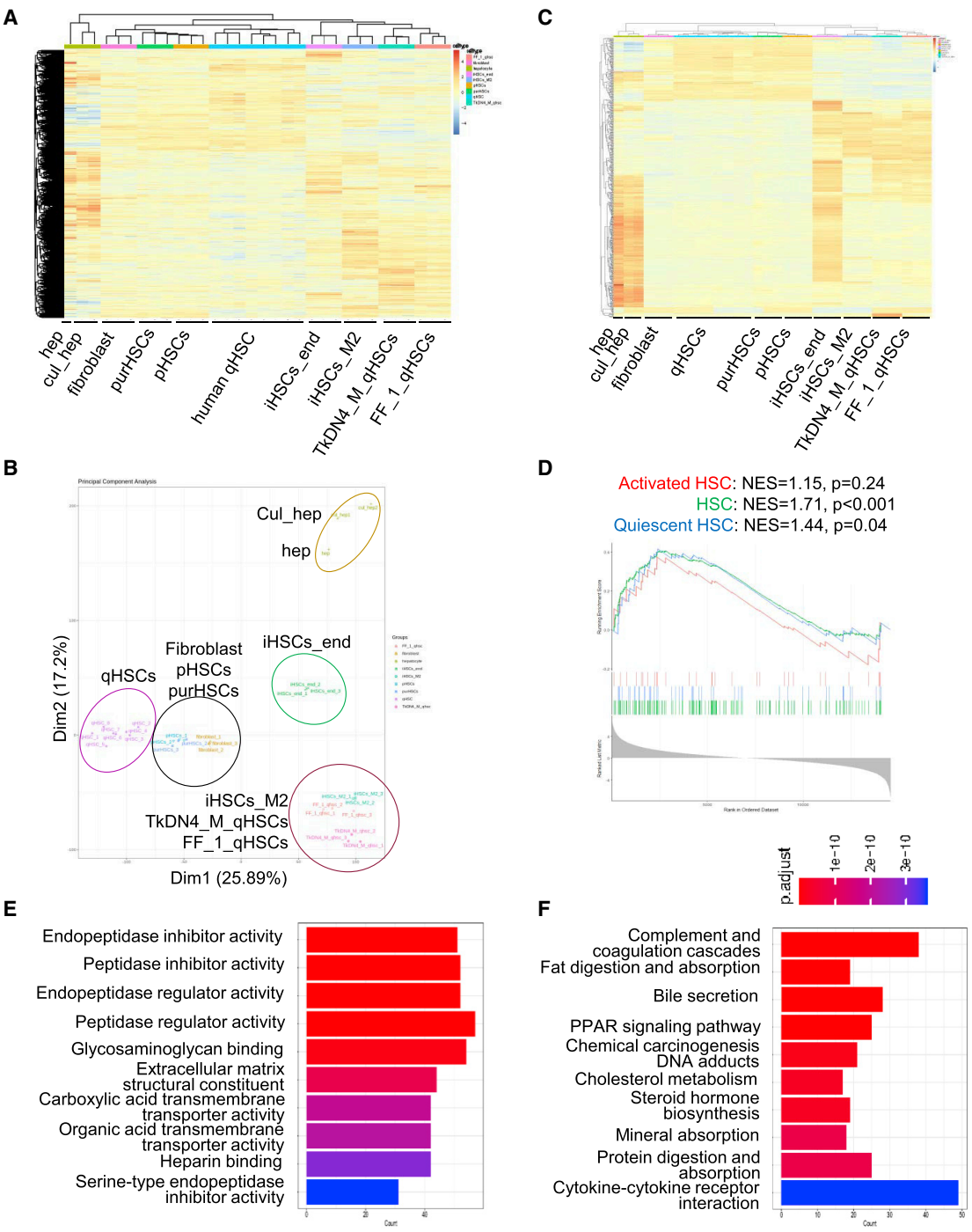

Figure 3. Transcriptomic comparison of iHSCs, qHSCs, pHSCs, and fibroblasts

(A) Representative heatmap of transcriptomic profiles of endoderm-derived iHSCs (iHSCs_end, n = 3) and mesoderm-derived iHSCs (iHSCs_M2, n = 3), purchased primary HSCs (purHSCs, n = 3), primary HSCs isolated from liver tissue (pHSC, n = 3), quiescent HSCs (qHSCs, n = 8) (GSE141100), iPSC-derived qHSCs (TkDN4_M_qHSCs, n = 3, and FF_1_qHSCs, n = 3) (GSE155017), human hepatocytes (hep, n = 1) (GSE43984), cultured hepatocytes (cul_hep, n = 2, GSE98710), and fibroblasts (n = 3).

(B) PCA of the transcriptomic comparison of endoderm-derived iHSCs (iHSCs_end, n = 3) and mesoderm-derived iHSCs (iHSCs_M2, n = 3), purchased primary HSCs (purHSCs, n = 3), primary HSCs purified from liver tissue (pHSC, n = 3), quiescent HSCs (qHSCs, n = 8) (GSE141100),

(legend continued on next page)

iHSCs (iHSCs_M2), purchased pHSCs (purHSCs) from Lonza, fibroblasts from Lonza, and pHSCs cultured for 4 days from liver isolation. Gene expression data of human qHSCs (Liu et al., 2020a) (GSE141100), hepatocytes (GSE43984), cultured hepatocytes (GSES98710) (Koui et al., 2017), and iPSC-derived qHSC-like cells (TkDN4_M_qHSCs and FF_1_qHSCs) (Koui et al., 2021) (GSE155017) were extracted from publicly available databases and processed for comparison. As shown in Figure 3A, the hierarchical clustering analysis demonstrated that the expression profile of iHSCs_end was similar to those of human qHSCs, TkDN4_M_qHSCs, and FF_1_qHSCs. It was reported that TkDN4_M_qHSCs and FF_1_qHSCs showed gene expression profiles similar to that of human qHSCs, which is rarely different in our analysis. Similarly, principal-component analysis (PCA) showed that there was a clear difference in gene expression profiles between iHSCs_end and pHSCs or fibroblasts (Figure 3B). However, human qHSCs, purHSCs, and pHSCs were clustered together with fibroblasts, suggesting that human qHSCs and pHSCs might have already been activated into myofibroblasts during the isolation or culture. In addition, to get more information on qHSC features, the 500 genes expressed differently between hepatocytes and different types of qHSCs were selected for further analysis. As shown in Figure 3C, the hierarchical clustering analysis showed that iHSCs_end presented a qHSC phenotype similar to those of TkDN4_M_qHSCs and FF_1_qHSCs.

We also performed gene set enrichment analysis (GSEA) based on the specific HSC gene signature as described previously (Coll et al., 2018; Wu et al., 2021). The signature genes highly expressed in HSCs are divided into three groups: HSC, qHSC, and aHSC signatures. The normalized enrichment score (NES) derived from the GSEA was 1.71 for HSC signature, 1.44 for qHSC signature, and 1.15 for aHSC signature (Figure 3D). In addition, gene ontology (GO) enrichment analysis and pathway analysis showed that nearly no fibrosis-related gene clusters were changed, but that extracellular matrix structural constituent and PPAR signaling pathway were significantly changed between iHSCs_end and TkDN4-M_qHSCs (Figures 3E and 3F). Table S1 shows the top downregulated genes in iHSCs compared with other cells. These data suggest that, although some gene expressions in iHSCs are different from those in qHSCs, iHSCs can still be considered as a close analog of qHSCs.

Activation of iHSCs derived from hESCs (H9) by stimulators

We next investigated the capability of iHSC activation after stimulation by TGF-β and fetal bovine serum (FBS) (Coll et al., 2018). As shown in Figure 4A, after 50 ng/mL TGF-β treatment for 5 days, a significant production of several fibrogenic and inflammatory markers (i.e., collagen I, α-SMA, and nestin) was detected in treated iHSCs. Similarly, more than 85% of cells treated with TGF-β (50 ng/mL) were collagen I and α-SMA positive (Figures 4B and S1E). Collagen I secretion significantly increased after 5 days of TGF-β (50 ng/mL) and 10% FBS (Figure 4C) treatment. We also did a time-course analysis of TGF-β treatment to stimulate iHSCs. As shown in Figure 4D, collagen I secretion did not increase after 2 days treatment, while it increased significantly after 4 days treatment. In addition, *COL1α1* and *ACTA2* transcripts were increased even at 5 ng/mL TGF-β treatment for 5 days (Figure 4E). It was reported that PDGF-BB could induce HSC migration (Coll et al., 2018). We also did a wound-healing assay to analyze the migration of iHSCs after PDGF-BB (20 ng/mL) and 10% FBS treatment. As shown in Figure 4F, both PDGF-BB and FBS increased the migration capacity of iHSCs and pHSCs, although the cell densities of iHSCs and pHSCs were different, resulting in different cell appearance.

The aforementioned iHSCs were differentiated from hESCs (H9). To further test the efficacy of this protocol, we also tested other stem cells, like hESCs (H1) and iPSCs. Apparently, iHSCs derived from hESCs (H1) showed mature HSC marker expression (i.e., desmin, PCDH7, and NCAM) (Figure S2A). After 5 days of 50 ng/mL TGF-β treatment (Figure S2B), HSC activation-related markers (e.g., collagen I, α-SMA, and nestin) were expressed (Figure S2C).

iPSC-derived qHSCs (TkDN4_M_qHSCs, n = 3, and FF_1_qHSCs, n = 3) (GSE155017), human hepatocytes (hep, n = 1) (GSE43984), cultured hepatocytes (cul_hep, n = 2, GSE98710), and fibroblasts (n = 3).

(C) Heatmap of the top 500 HSC genes expressed differently in endoderm-derived iHSCs (iHSCs_end, n = 3) and mesoderm-derived iHSCs (iHSCs_M2, n = 3), purchased primary HSCs (purHSCs, n = 3), primary HSCs purified from liver tissue (pHSC, n = 3), quiescent HSCs (qHSCs, n = 8) (GSE141100), iPSC-derived qHSCs (TkDN4_M_qHSCs, n = 3, and FF_1_qHSCs, n = 3) (GSE155017), human hepatocytes (hep, n = 1) (GSE43984), cultured hepatocytes (cul_hep, n = 2, GSE98710), and fibroblasts (n = 3).

(D) GSEA of the iHSC gene expression profile with qHSC and aHSC (GSE141100) gene signatures according to the phenotype described. NES, normalized enrichment score.

(E) GO analysis of 959 high-fold-change genes between iHSCs_end and TkDN4_M_qHSCs (GSE155017). The p values of the top 20 terms are indicated.

(F) Kyoto Encyclopedia of Genes and Genomes (KEGG) pathway analysis of 959 high-fold-change genes between endoderm-derived iHSCs (iHSCs_end) and other iPSCs derived qHSC-like cells from another laboratory (TkDNA4_M_qHSCs, GSE155017). The p values of enriched pathways are indicated. Data are represented as the mean ± SEM. See also Table S1.

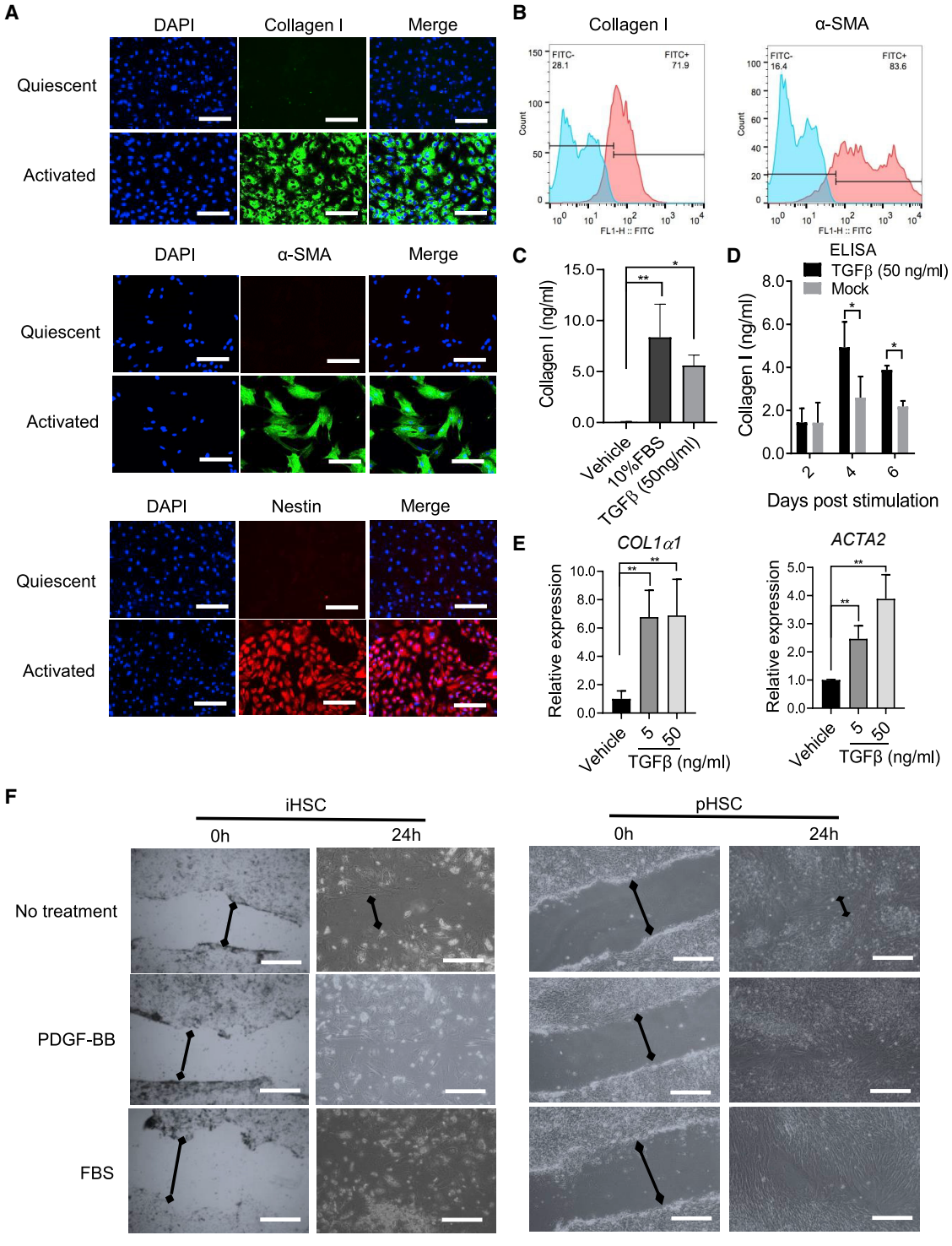

Figure 4. Activated HSC marker expression increases during activation as shown by functional analysis

The iHSCs were seeded in Matrigel-coated plates and activated by TGF-β (50 ng/mL) or 10% FBS in basal medium for 5 days. The related markers were detected by different assays.

(A) Representative images of collagen I, α-SMA, and nestin comparing quiescent iHSCs and iHSCs activated by TGF-β (50 ng/mL) for 5 days. Scale bars, 100 μm.

(legend continued on next page)

Moreover, we also generated similar quiescent iHSCs from iPSCs (Figures S3A–S3C) in the independent experiments, indicating the robustness of our protocol.

Toxicity assessment of iHSCs and HepaRG co-culture by thioacetamide and acetaminophen treatment

To further characterize iHSC functional fibrogenesis under the treatment of known drugs, the iHSCs were exposed to thioacetamide for 5 days (Coll et al., 2018). As expected, the exposure of iHSCs to 75 mM thioacetamide induced the expression of fibrogenic markers (*COL3α1*, *COL1α1*, and *ACTA2*). However, exposure of iHSCs to 25 mM thioacetamide did not display a fibrogenic response (Figure 5A), indicating that iHSC activation by thioacetamide is concentration dependent.

It was reported that acetaminophen needs to be metabolized by CYP2E1 and CYP3A4 into NAPQI in hepatocytes to be toxic to induce fibrogenic marker expression (Xie et al., 2014). To evaluate the potential use of iHSCs for toxicity assessment of acetaminophen, we co-cultured iHSCs with HepaRG cells in a Transwell system to mimic the interaction of hepatocytes and HSCs. HepaRG cells were seeded in the insert and iHSCs were seeded in the bottom well of the Transwell plate (Figure 5B). The HepaRG cells in the insert were exposed to acetaminophen for 5 days. As shown in Figure 5C, after treating the HepaRG cells in the co-culture system for 5 days, we found that acetaminophen stimulation induced concentration-dependent expression of fibrogenic markers. These results highlight the potential of iHSCs as an *in vitro* model for liver toxicity and fibrosis assessment.

HBV and HCV infection stimulate the activation of iHSCs

HBV and HCV infection could induce the activation of HSCs and further promote liver fibrogenesis (Akil et al., 2019; Bai et al., 2012; Pol et al., 2017; Revill et al., 2019). Han et al. reported a hepatocyte and HSC co-culture system to study the interaction between these cells (Han et al., 2021). To further evaluate the potential application of iHSCs for studying their activation by HBV and HCV infection, we designed experiments to co-culture iHSCs with HepG2-NTCP or Huh7.5 infected with HBV or HCV, respectively, in the Transwell system. Entecavir (ETV) treatment in the HBV infection system not only reduced HBV DNA and cccDNA levels, but also restricted HBsAg and HBeAg levels in the supernatant (Zhang et al., 2021). Thus, we used it as a control to inhibit HBV replication. As shown in Figure 6A, HepG2-NTCP cells were seeded in the inserts, then iHSCs were seeded in the bottom well of the Transwell plate. HepG2-NTCP cells were infected with 500 genome equivalents per cell (geq/cell) of HBV treated with or without 500 nM ETV. The co-culture was started after 1 day of HBV infection. The transcripts of fibrogenic markers were detected after 7 days of co-culture. Interestingly, consistent with another study (Bai et al., 2012), HBV infection could significantly stimulate the expression of fibrogenic markers such as *COL3α1*, *COL1α1*, and *ACTA2* in iHSCs, whereas inhibiting viral infection with ETV reduced related fibrogenic marker expression, as shown by the qPCR data (Figure 6B) and immunofluorescent staining results (Figure 6C). Just exposure of the iHSC and HepG2-NTCP co-culture system to ETV did not induce the increase in protein expression of collagen and α-SMA. Similar to the HBV infection experiments, HCV (MOI 10)-infected Huh7.5 cells were co-cultured with iHSCs in the Transwell system and treated with or without 700 nM sofosbuvir (SOF) for 3 days. HCV infection also induced the iHSC activation, as evidenced by the increased expression of fibrogenic markers (e.g., *COL3α1*, *COL1α1*, and *ACTA2*). After HCV infection was inhibited by SOF treatment, iHSCs showed low expression of fibrogenic markers as shown by the transcript (Figure 6D) and protein expression (Figure 6E) data. In addition, just exposing the cells to SOF did not induce fibrogenic marker expression, indicating that the decreased expression of fibrogenic markers was obtained by inhibiting HCV replication. Taken together, these results highlight the potential of iHSCs as an *in vitro* system of HSC activation by HBV and HCV infection. Antiviral therapy to restrict viral replication could attenuate the viral hepatitis-related HSC activation and further potential fibrogenesis.

Mesoderm- but not ectoderm-derived iHSCs can be obtained by this protocol

As reported previously, iHSCs were obtained from mesoderm-derived generation (Coll et al., 2018; Miyoshi et al.,

(B) Representative histograms of flow cytometric analysis of collagen I and α-SMA from quiescent iHSCs and iHSCs activated by TGF-β (50 ng/mL) for 5 days. Blue color means the isotype control and the red color means the tested markers' expression. See also Figure S1E.
(C) Comparison of collagen I expression between 10% FBS and TGF-β (50 ng/mL) treatment by ELISA; n = 3 in each group.
(D) ELISA of collagen I expression during the TGF-β (50 ng/mL) treatment from 2 to 6 days post activation; n = 3 in each group.
(E) qRT-PCR analysis of *COL1α1* and *ACTA2* expression during TGF-β treatment (5 and 50 ng/mL) for 5 days; n = 3 in each group.
(F) Representative images of the wound-healing assay, showing the scratch closure of iHSCs after incubation with PDGF-BB (20 ng/mL) or FBS (10%) for 24 h. Scale bars, 200 μm. Data are shown as the mean ± SEM from three independent experiments. The double-headed arrows means the distance of wound closure of iHSCs after incubation with PDGF-BB (20 ng/mL) or FBS (10%) for 24 h. Student's t test was used. *$p < 0.05$, **$p < 0.01$. See also Figures S2 and S3.

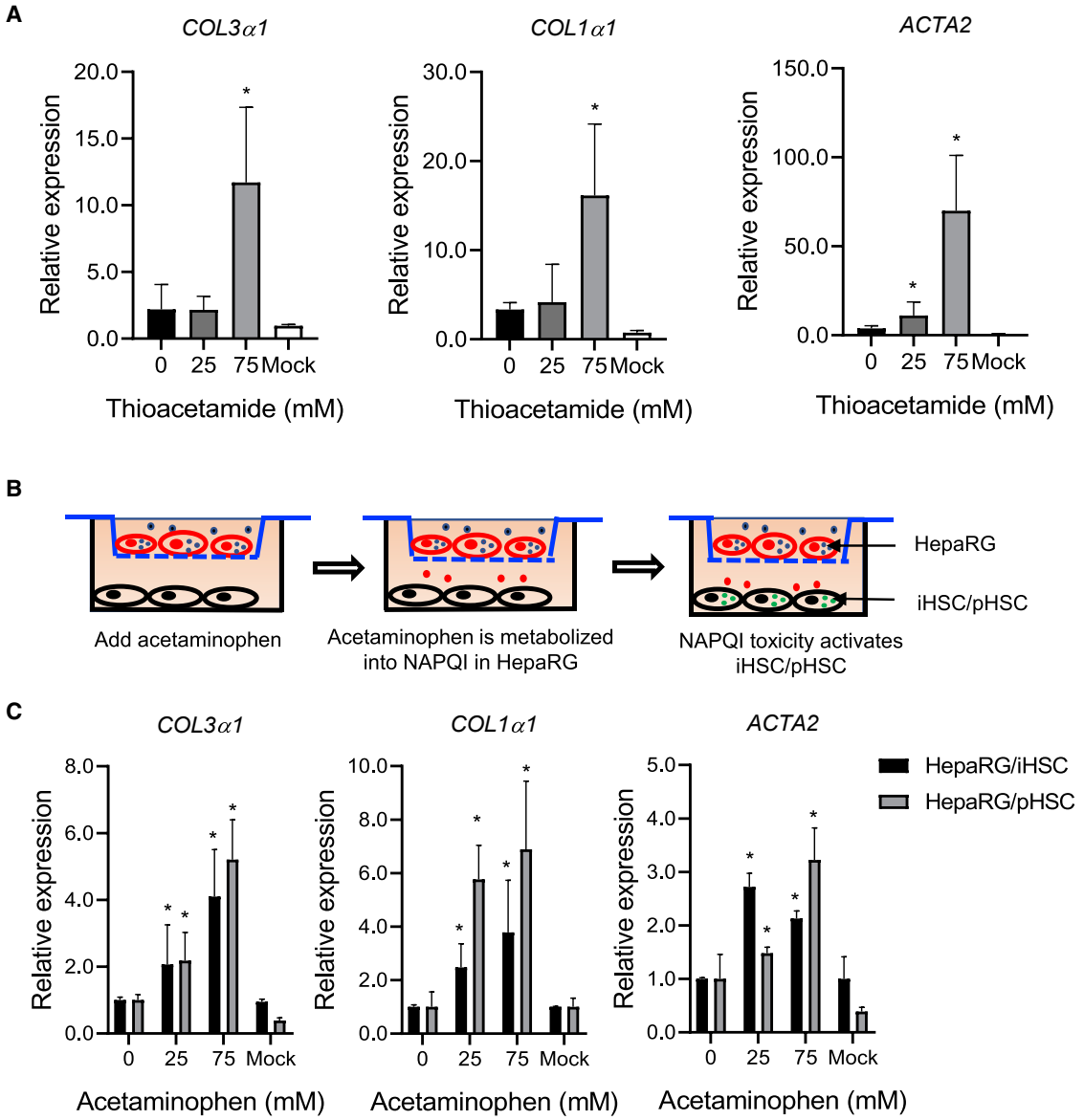

Figure 5. Fibrogenic and hepatocyte toxicity assays of thioacetamide and acetaminophen treatment stimulate iHSC activation

(A) qRT-PCR analysis of *COL3α1*, *COL1α1*, and *ACTA2* expression in iHSCs treated with thioacetamide for 5 days. The iHSCs were seeded in Matrigel-coated 24-well plates at a concentration of 80,000 cells per well on the first day. Then, the cells were treated with different concentrations of thioacetamide in basal medium for 5 days. qRT-PCR was performed to detect the activated iHSC-related markers; n = 3 in each group.

(B) Schematic representation of co-culture of iHSCs and HepaRG cells treated with acetaminophen for 5 days. The pHSC and HepaRG co-culture was performed as control.

(C) qRT-PCR analysis of *COL3α1*, *COL1α1*, and *ACTA2* expression in the iHSCs and pHSCs in the co-culture system shown in (B). qRT-PCR data are shown as the mean ± SEM from three independent experiments; n = 3 in each group. Student's t test was used. *p < 0.05.

2019). To test our protocol for mesoderm-derived differentiation, we first differentiated the hESCs (H9) into mesoderm. Then, the continued differentiation was performed using our established protocol (Figure 7A). Expression of HSC-related markers was successfully detected by flow cytometry (Figure 7B) and further confirmed by immunostaining (Figures 7C and S4A). Both PDGF-BB and FBS treatment increased the migration of activated iHSCs (Figure 7D). When the iHSCs_M2 were treated with injury-related mediator of TGF-β (5 or 50 ng/mL) in basal medium for 5 days (Figure 7E), the expression of aHSC markers (collagen I and α-SMA) was induced, while the

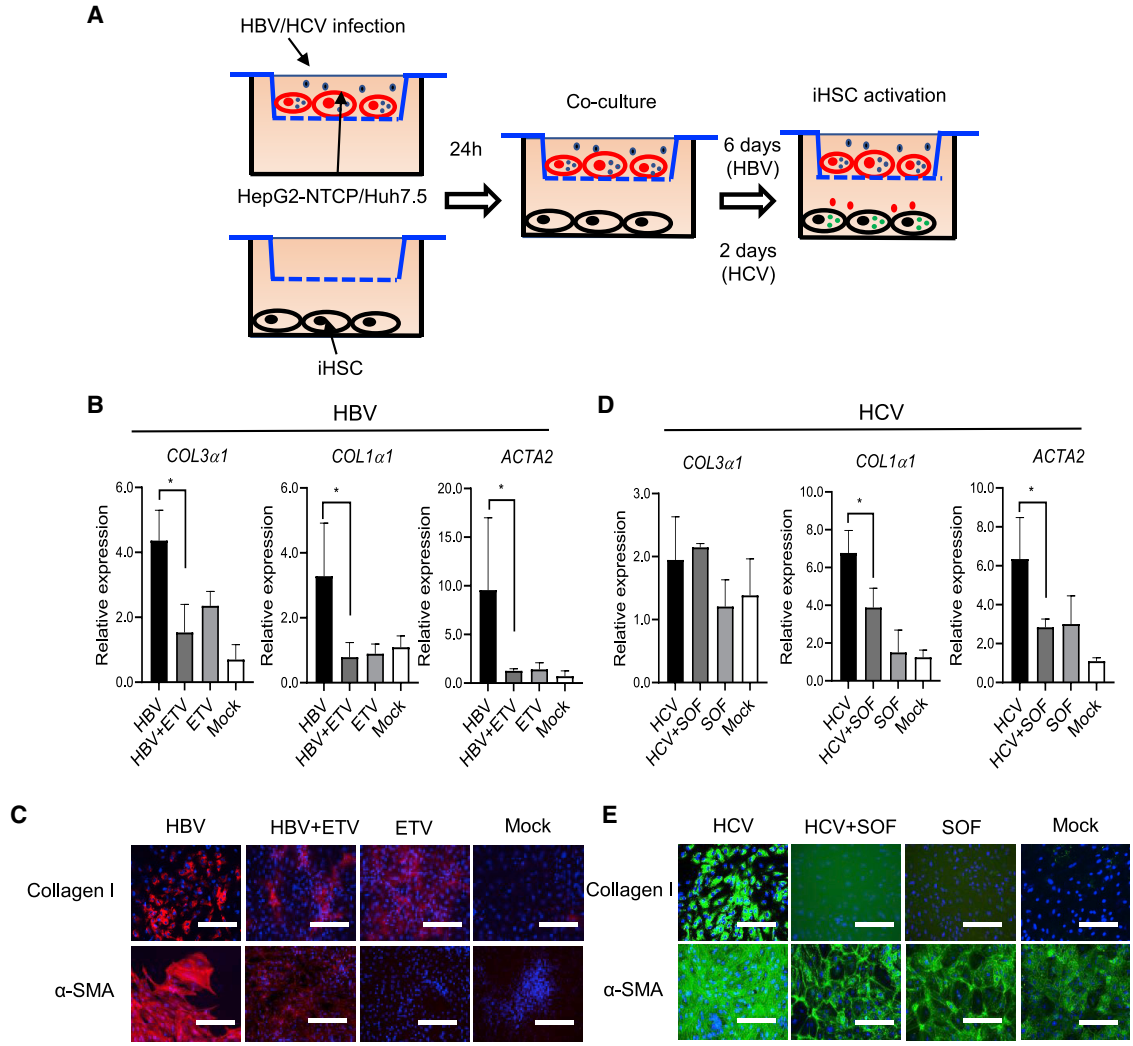

Figure 6. HBV and HCV infection and replication stimulate iHSC activation

(A) Schematic representation of HBV or HCV infection of hepatocytes co-cultured with iHSCs in the Transwell system.

(B) qRT-PCR analysis of *COL3α1*, *COL1α1*, and *ACTA2* expression in the co-culture of iHSCs and HBV (500 geq/cell)-infected HepG2-NTCP with or without ETV (500 nM) treatment for 7 days; n = 3 in each group.

(C) Representative images of collagen I and α-SMA in iHSCs during co-culture with HBV-infected HepG2-NTCP cells. Scale bars, 100 μm.

(D) qRT-PCR analysis of *COL3α1*, *COL1α1*, and *ACTA2* expression in the co-culture of iHSCs and HCV (MOI 10)-infected Huh7.5 cells with or without SOF (700 nM) for 3 days; n = 3 in each group.

(E) Representative images of collagen I and α-SMA in iHSCs during HCV infection. Scale bars, 100 μm. qRT-PCR data are shown as the mean ± SEM from three independent experiments. Student's t test was used. *p < 0.05.

HSC-related markers NCAM, desmin, and PCDH7 decreased during the TGF-β treatment (Figures 7F and 7G). Moreover, thioacetamide treatment stimulated iHSCs_M2 activation (Figure 7H), while acetaminophen did not show any influence (Figure 7I). In the Transwell system designed as shown in Figures 5B and 6A, acetaminophen treatment (Figure 7J) and HBV (Figure S4B) and HCV (Figure S4C) infection induced iHSC activation significantly. As shown in Figure S4D, most of the iHSC markers showed similar expression levels during passage, except for PPARγ, which showed significantly decreased expression during the subculture. To investigate the maintenance of iHSC functions during passage, we also did functional analysis on the iHSCs p2. As shown in Figures S4E and S4F, iHSC activation markers, such as *COL1α1*, *COL3α1*, and *ACTA2*, increased significantly after the treatments with TGF-β, FBS, and thioacetamide, suggesting that the passaged iHSCs also showed HSC characteristics. As shown in Figure 3A, the hierarchical clustering analysis demonstrated that the expression profile of iHSCs_M2 was also similar

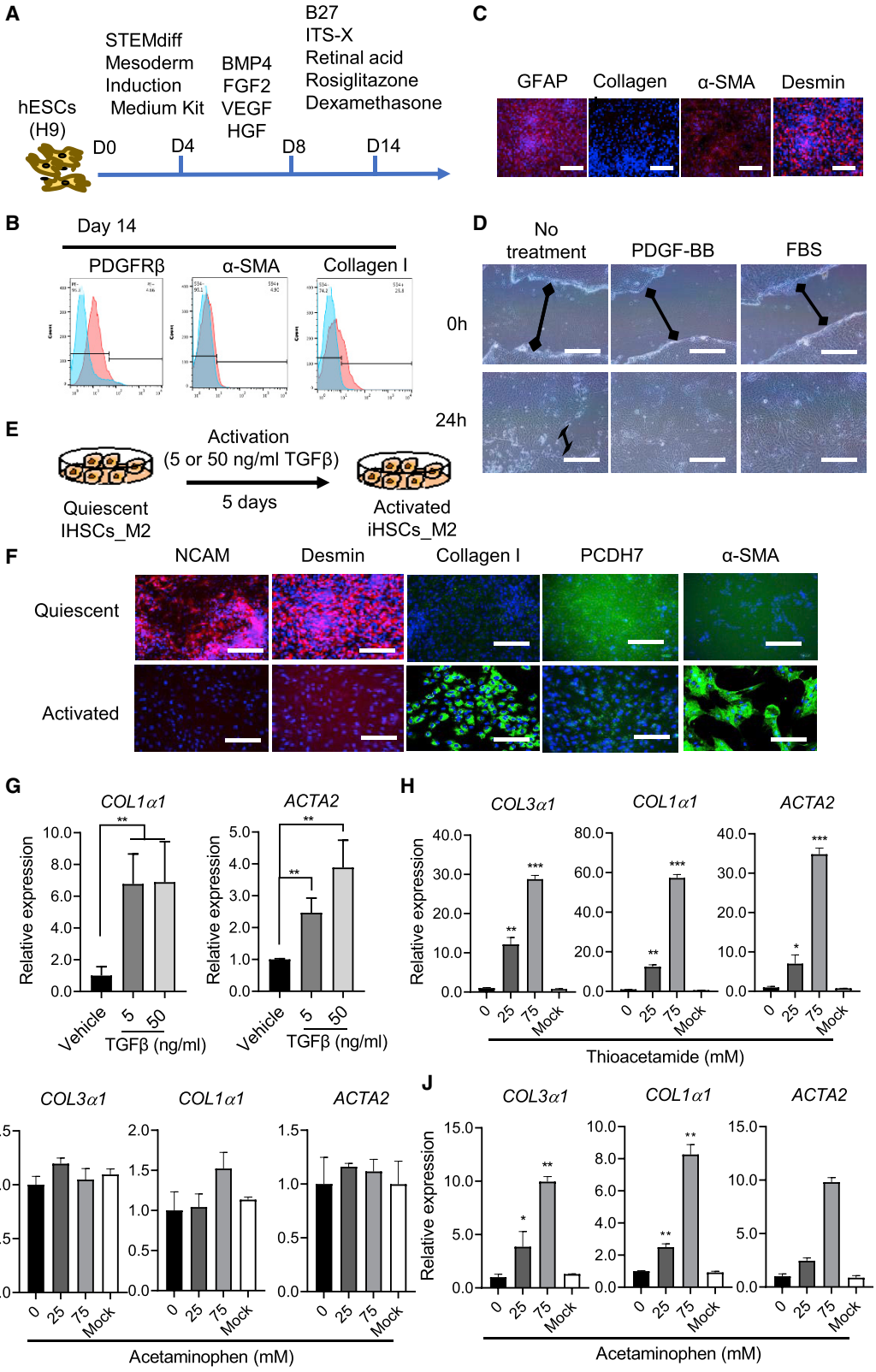

(legend on next page)

to those of TkDN4-M_qHSCs and FF-1_qHSCs. In addition, we also tested this protocol for ectoderm-derived differentiation. Unfortunately, although oil red staining showed some lipid droplet storage in the cells, the expression profile of ectoderm-derived differentiated cells was similar to that of the fibroblasts (Figures S5A–S5D).

Together, our results show that our protocol can differentiate hESCs or iPSCs into iHSCs through both endoderm and mesoderm pathways. This model offers a unique opportunity to study the mechanism of qHSC activation into aHSCs and fibrogenesis.

DISCUSSION

Studies on the mechanism of HSC activation in liver fibrogenesis are limited by the lack of an efficient *in vitro* cell culture system. In this study, we showed a novel and attractive lineage differentiation strategy to generate large quantities of functionally competent HSC-like cells from hESCs *in vitro*. The robust expansion capacity of the stem cells allows the generation of iHSC-like cells in large amounts, which provides an applicable *in vitro* cell model for the study of drug- and viral hepatitis-related fibrogenesis and anti-fibrosis drug discovery.

Compared with the traditional induction strategy, we demonstrated that the combination of key growth factors and compounds could be efficient to induce hESCs to directly differentiate into functionally competent HSC-like cells. Coll et al. reported that FGF2 could not induce hESCs into iHSCs (Coll et al., 2018). Another study showed that only BMP4 and FGF2 were sufficient to induce iHSCs (Miyoshi et al., 2019). In our study, we found that only BMP4 and FGF2 could not be sufficient to induce iHSC differentiation, which is consistent with the findings of Coll et al. (Coll et al., 2018). However, when inducing the hESCs with BMP4, FGF2, and additional VEGF, we could induce the cells to differentiate in the hESC direction. Interestingly, Koui et al. recently reported a similar strategy, in that BMP4, FGF2, and VEGF combined could induce iHSC differentiation, which supports that VEGF plays an important role in iHSC differentiation (Koui et al., 2021). In addition, PPARγ was discovered as a new transcription factor for regulating the phenotype of HSCs to prevent activation of HSCs, which could help us to maintain the qHSC features (Liu et al., 2020b). Thus, we further developed a mature iHSC medium using small molecules (rosiglitazone, retinal, and dexamethasone) (Liu et al., 2020b; Wu et al., 2018), which promoted the establishment of quiescent iHSCs with specific marker expression and vitamin A storage in the lipid droplets in the cells.

Importantly, to obtain functional qHSCs from the hESC and iPSC differentiation, it is pivotal to devise culture conditions to promote terminal differentiation of HSC-like cells. Our strategy for the maturation medium was developed based on conditions that retinal acid promotes cells to store vitamin A in the lipid droplets and rosiglitazone maintains the quiescent phenotype of HSCs (Liu et al., 2020b). Using this procedure, the cells acquired mature HSC properties in terms of HSC morphology, key HSC marker expression, and basic HSC functions. Moreover, the transcriptional profile of iHSCs accumulated nearly to that of qHSCs but with some differences. The pHSCs were already activated during the isolation and culture; some of them even activated in the tissue, which showed gene expression similar to that of aHSCs and fibroblasts. However, combined with other data, our iHSC-like cells more resemble qHSCs, indicating that this procedure promotes mature and quiescent iHSC differentiation (Coll et al., 2018; Koui et al., 2021). In addition, the acquisition of a mature state by iHSCs in the differentiation medium was characterized by the wound-healing response after TGF-β treatment.

Figure 7. Characterization of the activation of mesoderm-derived iHSCs

(A) Schematic representation of the differentiation protocol from mesoderm to iHSCs.

(B) Representative histograms of flow cytometric analysis of different markers' expression in quiescent iHSCs (PDGFRβ) and activated iHSCs (α-SMA and collagen I). Positive gates were defined based on the isotype control. Blue color means the isotype control and the red color means the tested markers' expression.

(C) Immunostaining analysis was performed to detect HSC-related markers (GFAP, collagen I, α-SMA, and desmin). Scale bars, 100 μm.

(D) Representative images of the wound-healing assay, showing the scratch closure of iHSCs after incubation with PDGFR-BB (20 ng/mL) and FBS (10%) for 24 h. The double-headed arrows means the distance of wound closure of iHSCs after incubation with PDGF-BB (20 ng/mL) or FBS (10%) for 24 h. Scale bars, 200 μm.

(E) Schematic representation of the activation of mesoderm-derived iHSCs by TGF-β (50 ng/mL) in basal medium for 5 days.

(F) Immunostaining analysis of HSC markers (NCAM, desmin, PCDH7) and aHSC markers (collagen I and α-SMA). Scale bars, 100 μm.

(G) Activated HSC gene expression of *COL1α1* and *ACTA2* by TGF-β treatment was assessed by qPCR; n = 3 in each group.

(H and I) Activated HSC gene expression of *COL3α1*, *COL1α1*, and *ACTA2* by thioacetamide and acetaminophen, respectively, was assessed by qPCR; n = 3 in each group.

(J) In the Transwell system with HepaRG and iHSC co-culture, activated HSC gene expression of *COL3α1*, *COL1α1*, and *ACTA2* by acetaminophen was assessed by qPCR; n = 3 in each group. Data are shown as the mean ± SEM from three independent experiments. Student's t test was used. *p < 0.05, **p < 0.01, ***p < 0.001. See also Figure S4.

Hepatic fibrosis is a dynamic process characterized by HSC activation from *trans*-differentiation of quiescent, vitamin A-storing cells into proliferative, fibrogenic myofibroblasts during liver injury (Tsuchida and Friedman, 2017). Thus, it is very important to have a cell model to mimic this dynamic process. Although pHSCs and other iHSCs in the published protocol could express collagen I and α-SMA during drug stimulation and viral infection, these cells were already activated with collagen I and α-SMA (Coll et al., 2018). In addition, the limited sources and restricted accessibility of pHSCs make them difficult to apply at a large scale for high-throughput applications and mechanism studies of HSC activation as well (Shang et al., 2018). The most important feature on the applied side of our work is that iHSCs have quiescent features, which could mimic the activation process of HSCs from qHSCs to aHSCs. Compared with previous studies, the iHSCs differentiated by our new strategy are similar in terms of morphology, gene expression patterns, and functionality to qHSCs (Coll et al., 2018). Importantly, iHSCs from our protocol are more quiescent than others, and showed almost no collagen I and α-SMA expression in the quiescent iHSCs, but nearly all cells showed high expression during activation (Coll et al., 2018; Koui et al., 2021). These data suggest that iHSCs generated by our strategy are promising for large-scale applications and mechanism studies of HSC activation *in vitro* and may resolve the shortage of activation phenotype of pHSCs.

Our *in vitro*-generated iHSCs efficiently recapitulated quiescent iHSC functionality, particularly responses to liver-toxic drugs and viral infection such as HBV and HCV. Thioacetamide could directly stimulate iHSC activation, and acetaminophen should be metabolized by CYP2E1 and CYP3A4 into NAPQI in hepatocytes to be toxic enough to stimulate iHSC activation, resulting in collagen I and α-SMA expression (Xie et al., 2014). HBV and HCV infection can induce the activation of HSCs to fibrogenesis, while cure of HBV and HCV infection has been shown to reduce the advanced fibrosis and risk of HCC (Bataller et al., 2004; Gong et al., 2016; Kanwal et al., 2017, 2020; Liu et al., 2009). In our study, hepatocytes co-cultured with iHSCs that were infected with HBV and HCV could also induce iHSC activation (Figure 6), while the iHSC activation could be attenuated by antiviral treatment, indicating that inhibition of viral replication evidently reduces the fibrogenesis. These data highlight the potential of iHSCs in place of pHSCs in toxicity assessment, fibrogenesis study, and anti-liver-fibrosis drug screening at a large scale.

In addition, our differentiation strategy provides a useful model to study the detailed mechanisms of human HSC development. It is still unclear which cell type is the embryonic origin of human HSCs. Recent studies based on cell-fate mapping in mice showed that HSCs might originate from the septum transversum (Shang et al., 2018). Others have speculated that HSCs might originate from endoderm, mesoderm-derived septum transversum mesenchyme, or the neural crest based on the expression markers (Shang et al., 2018). In addition, recent studies, which utilized stem cell differentiation technology to induce iHSCs_M2, suggested that HSCs originate from the mesoderm (Coll et al., 2018; Koui et al., 2021; Shang et al., 2018). Interestingly, our strategy could induce both hESC-derived mesoderm and endoderm cells into iHSCs, rather than ectoderm cells, which provided evidence that the origin of human HSCs might be derived from both endoderm and mesoderm in the early developmental stages of the human embryo (Friedman, 2008; Geerts, 2004). Thus, our results indicate that iHSCs could potentially be induced from both endoderm and mesoderm, which provides a useful *in vitro* model to further study the possible molecular regulation mechanisms of HSCs.

In a recent study, Koui et al. reported a new protocol for qHSC differentiation. They showed that the factors FGF2 + BMP4 + VEGF combine to induce iPSCs sourced from mesoderm into qHSCs, which could be converted into aHSCs in culture (Koui et al., 2021). However, their work was based on others' work to optimize the protocol to induce mesoderm into qHSCs. In this study, our protocol not only could differentiate the mesoderm into qHSCs, but also could differentiate the endoderm into qHSCs, which has not been reported elsewhere and will be helpful in studying the embryonic origin of HSCs. Moreover, the endoderm-derived qHSCs showed most of the cells having vitamin A droplets with almost no collagen I or α-SMA expression by our protocol. And more than 80% of the cells expressed collagen I and α-SMA after activation (Figure 4). In addition, our established qHSCs could be used not only to study drug toxicity, but also to study the mechanisms of viral infection-caused HSC activation. Antiviral treatment could reduce viral infection-caused HSC activation.

In conclusion, iHSCs were established through hESC and iPSC differentiation, displaying functional and phenotypic features of quiescent human primary cultured HSCs. The co-culture of iHSCs and hepatocytes in a Transwell system could also mimic drug toxicity and viral hepatitis-caused liver fibrosis of iHSC activation. This cell model may be a novel and robust resource for human HSCs for viral hepatitis-based and anti-liver-fibrosis drug screening studies.

EXPERIMENTAL PROCEDURES

Human ESC and iPSC culture

The hESC lines WA09 (H9) and WA01 (H1) (WiCell Research Institute, USA) obtained from female embryonic stem cells and iPSCs (Cauliscell, USA) were cultured on growth-factor-reduced Matrigel

according to the manufacturer's recommendation in mTeSR1 medium. The cells were replenished with fresh medium every day. All the cells in this study were used between passages 35 and 50.

Isolation of HSCs

The pHSCs were obtained from non-tumor liver tissue harvested during liver transplantation and cirrhotic liver tissue at the Youan Hospital and First Medical Center of Chinese PLA General Hospital, Beijing, China. All samples were collected with informed consent from patients. The isolation of HSCs was performed as described previously (Coll et al., 2015; Perea et al., 2015). Briefly, liver samples were treated by mechanical homogenization and then digested with enzymatic solution 1 (Gey's balanced salt solution [GBSS] [Sigma, USA] containing 3.15 mg/mL Pronase [Roche, USA], 0.38 mg/mL collagenase A [Roche, USA], 0.01 mg/mL DNase I [Roche, USA]) and then enzymatic solution 2 (GBSS with 0.6 mg/mL Pronase [Roche, USA], 0.38 mg/mL collagenase A, 0.01 mg/mL DNase I) at 37°C for 30 min. HSCs were isolated from cell suspension with 9% Nycodenz (Sigma, USA). The pHSCs obtained from the cell fraction were cultured in DMEM GlutaMax (GIBCO, USA) supplemented with 10% FBS (GIBCO, USA) and 1% penicillin-streptomycin (Sigma, USA) and used until passage 6.

Differentiation into three germ layers

For endoderm, hESCs (H9 and H1) and human iPSCs were dissociated into single cells using Accutase and plated in the Matrigel-coated plates with 10 μM ROCK inhibitor (Y-27632). Differentiation was induced by using the STEMdiff definitive endoderm kit following the manufacturer's instructions (Wu et al., 2018).

For mesoderm, differentiation of hESCs (H9 and H1) and human iPSCs into mesoderm was performed accordingly. Briefly, hESCs (H9 and H1) and human iPSCs were dissociated into single cells using Accutase and plated onto Matrigel-coated plates with ROCK inhibitor (Y27632) to reach approximately 60% confluence. Differentiation was induced by the STEMdiff mesoderm induction medium kit following the manufacturer's instructions (Wu et al., 2018).

For ectoderm, hESCs (H9 and H1) and human iPSCs were differentiated into neuroectoderm cells as described previously. Briefly, hESCs (H9 and H1) and human iPSCs were seeded at 1×10^5 cells/cm^2 and cultured in mTeSR1 medium with ROCK inhibitor (Y27632). The next day, the cells were differentiated with SRM (DMEM/F12, 10% knockout serum replacement [KOSR], and 1% GlutaMax) supplemented with 10 μM SB431542 and 200 nM Noggin for 5 days (Wu et al., 2018).

HSC differentiation

For HSC specification, endoderm or mesoderm was dissociated into single cells using Accutase and plated onto Matrigel-coated plates with ROCK inhibitor in basal medium (BM; DMEM/F12 + 10% KOSR +1% GlutaMax +1% penicillin-streptomycin; Life Technologies, USA) supplemented with 10 ng/mL FGF2 (Peprotech, USA), 5 ng/mL BMP4 (R&D, USA), 10 ng/mL VEGF (Peprotech, USA), and 10 ng/mL HGF (Peprotech, USA). The medium was replaced every 2 days for 4 days. Then, the cells were exposed to BM containing 1× B27 (Life Technologies, USA), 1× insulin-transferrin-selenium-ethanolamine (ITS-X; Life Technologies, USA), 1 μM retinoic acid (RA; Sigma-Aldrich, USA), 20 μM rosiglitazone (Selleck Chemicals, USA), and 2.5 μM dexamethasone (Sigma-Aldrich, USA) for 6 days. Differentiated HSCs could then be maintained in the BM containing 1× B27, 1× ITS-X, 1 μM RA, 20 μM rosiglitazone, and 2.5 μM dexamethasone, with the medium changed twice per week.

Ethics approval and consent to participate

Informed consents were obtained regarding the use of samples for further studies. This study was approved by the ethics committees of the Medical Center of Chinese PLA General Hospital, Beijing, China (S2018-111-01).

Statistical analysis

Every experiment was repeated at least three times. Data are shown as means ± SEM and were analyzed using an unpaired Student t test or Mann-Whitney U test when appropriate (GraphPad Software v.8). Values of $p < 0.05$ were considered as statistically significant.

Resource availability

Corresponding author

Further information and requests for resources and reagents should be directed to and will be fulfilled by the corresponding author, Kuanhui Xiang (kxiang@bjmu.edu.cn).

Materials availability

All materials in this study are available from the Lead Contact with a completed Materials Transfer Agreement.

Data and code availability

The transcriptomic data generated during this study are available at NCBI (SRA: PRJNA727427)

SUPPLEMENTAL INFORMATION

Supplemental information can be found online at https://doi.org/10.1016/j.stemcr.2022.09.010.

AUTHOR CONTRIBUTIONS

K.X., Y.S., T.L., and H.Z. designed the research; X.L., C.L., K.Z., C.X., J.C., J.S., and B.X. collected the tissue samples; K.X., X.L., C.L., C.X., K.Z., L.W., B.X., J.C., J.S., and J.D. performed the experiments; K.X., Y.S., H.Z., Z.P., and T.L. analyzed the data; K.X., Y.S., T.L., H.D., S.L., and H.Z. wrote and revised the manuscript.

ACKNOWLEDGMENTS

This work was funded by The National Natural Science Foundation of China (grants 81873579 and 81802002 to K.X. and 81772174 to T.L.), the Excellent Ph.D. Cultivation Project of Peking University Health Science Center (grant BMU2017YB001 to K.X.), the Major Science and Technology Special Project of China Thirteenth Five-Year Plan (2017ZX10202202-004-004 to T.L.), and the Beijing Key Laboratory of Emerging Infectious Diseases (DTKF202101 to K.X.). We gratefully thank Charles M. Rice (The Rockefeller University) for providing the Huh7.5 and HepG2-NTCP cells. We thank Dr. Xianfang Wu (The Cleveland Clinic) for helpful discussion.

CONFLICT OF INTERESTS

The authors declare no competing interests.

Received: February 16, 2022
Revised: September 23, 2022
Accepted: September 26, 2022
Published: October 20, 2022

REFERENCES

Ajat, M., Molenaar, M., Brouwers, J.F.H.M., Vaandrager, A.B., Houweling, M., and Helms, J.B. (2017). Hepatic stellate cells retain the capacity to synthesize retinyl esters and to store neutral lipids in small lipid droplets in the absence of LRAT. Biochim. Biophys. Acta. Mol. Cell Biol. Lipids *1862*, 176–187.

Akil, A., Endsley, M., Shanmugam, S., Saldarriaga, O., Somasunderam, A., Spratt, H., Stevenson, H.L., Utay, N.S., Ferguson, M., and Yi, M. (2019). Fibrogenic gene expression in hepatic stellate cells induced by HCV and HIV replication in a three cell co-culture model system. Sci. Rep. *9*, 568.

Asrani, S.K., Devarbhavi, H., Eaton, J., and Kamath, P.S. (2019). Burden of liver diseases in the world. J. Hepatol. *70*, 151–171.

Bai, Q., An, J., Wu, X., You, H., Ma, H., Liu, T., Gao, N., and Jia, J. (2012). HBV promotes the proliferation of hepatic stellate cells via the PDGF-B/PDGFR-β signaling pathway in vitro. Int. J. Mol. Med. *30*, 1443–1450.

Bataller, R., Paik, Y.H., Lindquist, J.N., Lemasters, J.J., and Brenner, D.A. (2004). Hepatitis C virus core and nonstructural proteins induce fibrogenic effects in hepatic stellate cells. Gastroenterology *126*, 529–540.

Coll, M., El Taghdouini, A., Perea, L., Mannaerts, I., Vila-Casadesús, M., Blaya, D., Rodrigo-Torres, D., Affò, S., Morales-Ibanez, O., Graupera, I., et al. (2015). Integrative miRNA and gene expression profiling analysis of human quiescent hepatic stellate cells. Sci. Rep. *5*, 11549.

Coll, M., Perea, L., Boon, R., Leite, S.B., Vallverdú, J., Mannaerts, I., Smout, A., El Taghdouini, A., Blaya, D., Rodrigo-Torres, D., et al. (2018). Generation of hepatic stellate cells from human pluripotent stem cells enables in vitro modeling of liver fibrosis. Cell Stem Cell *23*, 101–113.e7.

Friedman, S.L. (2008). Hepatic stellate cells: protean, multifunctional, and enigmatic cells of the liver. Physiol. Rev. *88*, 125–172.

Geerts, A. (2004). On the origin of stellate cells: mesodermal, endodermal or neuro-ectodermal? J. Hepatol. *40*, 331–334.

Gong, J., Tu, W., Han, J., He, J., Liu, J., Han, P., Wang, Y., Li, M., Liu, M., Liao, J., et al. (2016). Hepatic SATB1 induces paracrine activation of hepatic stellate cells and is upregulated by HBx. Sci. Rep. *6*, 37717.

Gutierrez-Ruiz, M.C., and Gomez-Quiroz, L.E. (2007). Liver fibrosis: searching for cell model answers. Liver Int. *27*, 434–439.

Han, B., Mo, H., Svarovskaia, E., and Mateo, R. (2021). A primary human hepatocyte/hepatic stellate cell co-culture system for improved in vitro HBV replication. Virology *559*, 40–45.

Iacob, R., Rüdrich, U., Rothe, M., Kirsch, S., Maasoumy, B., Narain, N., Verfaillie, C.M., Sancho-Bru, P., Iken, M., Popescu, I., et al. (2011). Induction of a mature hepatocyte phenotype in adult liver derived progenitor cells by ectopic expression of transcription factors. Stem Cell Res. *6*, 251–261.

Jin, X., Aimaiti, Y., Chen, Z., Wang, W., and Li, D. (2018). Hepatic stellate cells promote angiogenesis via the TGF-beta1-Jagged1/VEGFA axis. Exp. Cell Res. *373*, 34–43.

Kanwal, F., Kramer, J., Asch, S.M., Chayanupatkul, M., Cao, Y., and El-Serag, H.B. (2017). Risk of hepatocellular cancer in HCV patients treated with direct-acting antiviral agents. Gastroenterology *153*, 996–1005.e1.

Kanwal, F., Kramer, J.R., Asch, S.M., Cao, Y., Li, L., and El-Serag, H.B. (2020). Long-term risk of hepatocellular carcinoma in HCV patients treated with direct acting antiviral agents. Hepatology *71*, 44–55.

Kawada, N., Kristensen, D.B., Asahina, K., Nakatani, K., Minamiyama, Y., Seki, S., and Yoshizato, K. (2001). Characterization of a stellate cell activation-associated protein (STAP) with peroxidase activity found in rat hepatic stellate cells. J. Biol. Chem. *276*, 25318–25323.

Koui, Y., Kido, T., Ito, T., Oyama, H., Chen, S.W., Katou, Y., Shirahige, K., and Miyajima, A. (2017). An in vitro human liver model by iPSC-derived parenchymal and non-parenchymal cells. Stem Cell Rep. *9*, 490–498.

Koui, Y., Himeno, M., Mori, Y., Nakano, Y., Saijou, E., Tanimizu, N., Kamiya, Y., Anzai, H., Maeda, N., Wang, L., et al. (2021). Development of human iPSC-derived quiescent hepatic stellate cell-like cells for drug discovery and in vitro disease modeling. Stem Cell Rep. *16*, 3050–3063.

Liu, X., Zhu, S.T., You, H., Cong, M., Liu, T.H., Wang, B.E., and Jia, J.D. (2009). Hepatitis B virus infects hepatic stellate cells and affects their proliferation and expression of collagen type I. Chin. Med. J. *122*, 1455–1461.

Liu, X., Rosenthal, S.B., Meshgin, N., Baglieri, J., Musallam, S.G., Diggle, K., Lam, K., Wu, R., Pan, S.Q., Chen, Y., et al. (2020a). Primary alcohol-activated human and mouse hepatic stellate cells share similarities in gene-expression profiles. Hepatol. Commun. *4*, 606–626.

Liu, X., Xu, J., Rosenthal, S., Zhang, L.J., McCubbin, R., Meshgin, N., Shang, L., Koyama, Y., Ma, H.Y., Sharma, S., et al. (2020b). Identification of lineage-specific transcription factors that prevent activation of hepatic stellate cells and promote fibrosis resolution. Gastroenterology *158*, 1728–1744.e14.

Mederacke, I., Dapito, D.H., Affò, S., Uchinami, H., and Schwabe, R.F. (2015). High-yield and high-purity isolation of hepatic stellate cells from normal and fibrotic mouse livers. Nat. Protoc. *10*, 305–315.

Miyoshi, M., Kakinuma, S., Kamiya, A., Tsunoda, T., Tsuchiya, J., Sato, A., Kaneko, S., Nitta, S., Kawai-Kitahata, F., Murakawa, M., et al. (2019). LIM homeobox 2 promotes interaction between human iPS-derived hepatic progenitors and iPS-derived hepatic stellate-like cells. Sci. Rep. *9*, 2072.

Perea, L., Coll, M., and Sancho-Bru, P. (2015). Assessment of liver fibrotic insults in vitro. Methods Mol. Biol. *1250*, 391–401.

Pol, S., Haour, G., Fontaine, H., Dorival, C., Petrov-Sanchez, V., Bourliere, M., Capeau, J., Carrieri, P., Larrey, D., Larsen, C., et al.

(2017). The negative impact of HBV/HCV coinfection on cirrhosis and its consequences. Aliment. Pharmacol. Ther. *46*, 1054–1060.

Revill, P.A., Chisari, F.V., Block, J.M., Dandri, M., Gehring, A.J., Guo, H., Hu, J., Kramvis, A., Lampertico, P., Janssen, H.L.A., et al. (2019). A global scientific strategy to cure hepatitis B. Lancet. Gastroenterol. Hepatol. *4*, 545–558.

Roehlen, N., Crouchet, E., and Baumert, T.F. (2020). Liver fibrosis: mechanistic concepts and therapeutic perspectives. Cells *9*, 875.

Shang, L., Hosseini, M., Liu, X., Kisseleva, T., and Brenner, D.A. (2018). Human hepatic stellate cell isolation and characterization. J. Gastroenterol. *53*, 6–17.

Theis, V., and Theiss, C. (2018). VEGF - a stimulus for neuronal development and regeneration in the CNS and PNS. Curr. Protein Pept. Sci. *19*, 589–597.

Tsuchida, T., and Friedman, S.L. (2017). Mechanisms of hepatic stellate cell activation. Nat. Rev. Gastroenterol. Hepatol. *14*, 397–411.

Wang, C., Sun, X., Miao, Z., Lv, Y., Yang, Y., Zhang, H., Zhang, P., Liu, Y., Du, L., Gao, Y., et al. (2012). TGFβ inhibition enhances the generation of hematopoietic progenitors from human ES cell-derived hemogenic endothelial cells using a stepwise strategy. Cell Res. *22*, 194–207.

Wu, X., Dao Thi, V.L., Huang, Y., Billerbeck, E., Saha, D., Hoffmann, H.H., Wang, Y., Silva, L.A.V., Sarbanes, S., Sun, T., et al. (2018). Intrinsic immunity shapes viral resistance of stem cells. Cell *172*, 423–438.e25.

Wu, T., Hu, E., Xu, S., Chen, M., Guo, P., Dai, Z., Feng, T., Zhou, L., Tang, W., Zhan, L., et al. (2021). clusterProfiler 4.0: a universal enrichment tool for interpreting omics data. Innovation *2*, 100141.

Xie, Y., McGill, M.R., Dorko, K., Kumer, S.C., Schmitt, T.M., Forster, J., and Jaeschke, H. (2014). Mechanisms of acetaminophen-induced cell death in primary human hepatocytes. Toxicol. Appl. Pharmacol. *279*, 266–274.

Xu, L., Hui, A.Y., Albanis, E., Arthur, M.J., O'Byrne, S.M., Blaner, W.S., Mukherjee, P., Friedman, S.L., and Eng, F.J. (2005). Human hepatic stellate cell lines, LX-1 and LX-2: new tools for analysis of hepatic fibrosis. Gut *54*, 142–151.

Zhang, K., Lai, X., Song, J., He, L., Wang, L., Ou, G., Tian, X., Wang, L., Deng, J., Zhang, J., et al. (2021). A novel cell culture model reveals the viral interference during hepatitis B and C virus coinfection. Antivir. Res. *189*, 105061.

Stem Cell Reports, Volume *17*

Supplemental Information

Generation of functionally competent hepatic stellate cells from human stem cells to model liver fibrosis *in vitro*

Xinyuan Lai, Chuanyun Li, Chengang Xiang, Zihang Pan, Kai Zhang, Lei Wang, Bingqing Xie, Junning Cao, Jihang Shi, Juan Deng, Shichun Lu, Hongkui Deng, Hui Zhuang, Tong Li, Yan Shi, and Kuanhui Xiang

Supplemental Information

Generation of functionally competent hepatic stellate cells from human stem cells to model liver fibrosis *in vitro*

Xinyuan Lai, Chuanyun Li, Chengang Xiang, Zihang Pan, Kai Zhang, Lei Wang, Bingqing Xie, Junning Cao, Jihang Shi, Juan Deng, Shichun Lu, Hongkui Deng, Hui Zhuang, Tong Li, Yan Shi, Kuanhui Xiang

Supplementary figures and Legends

Figure S1

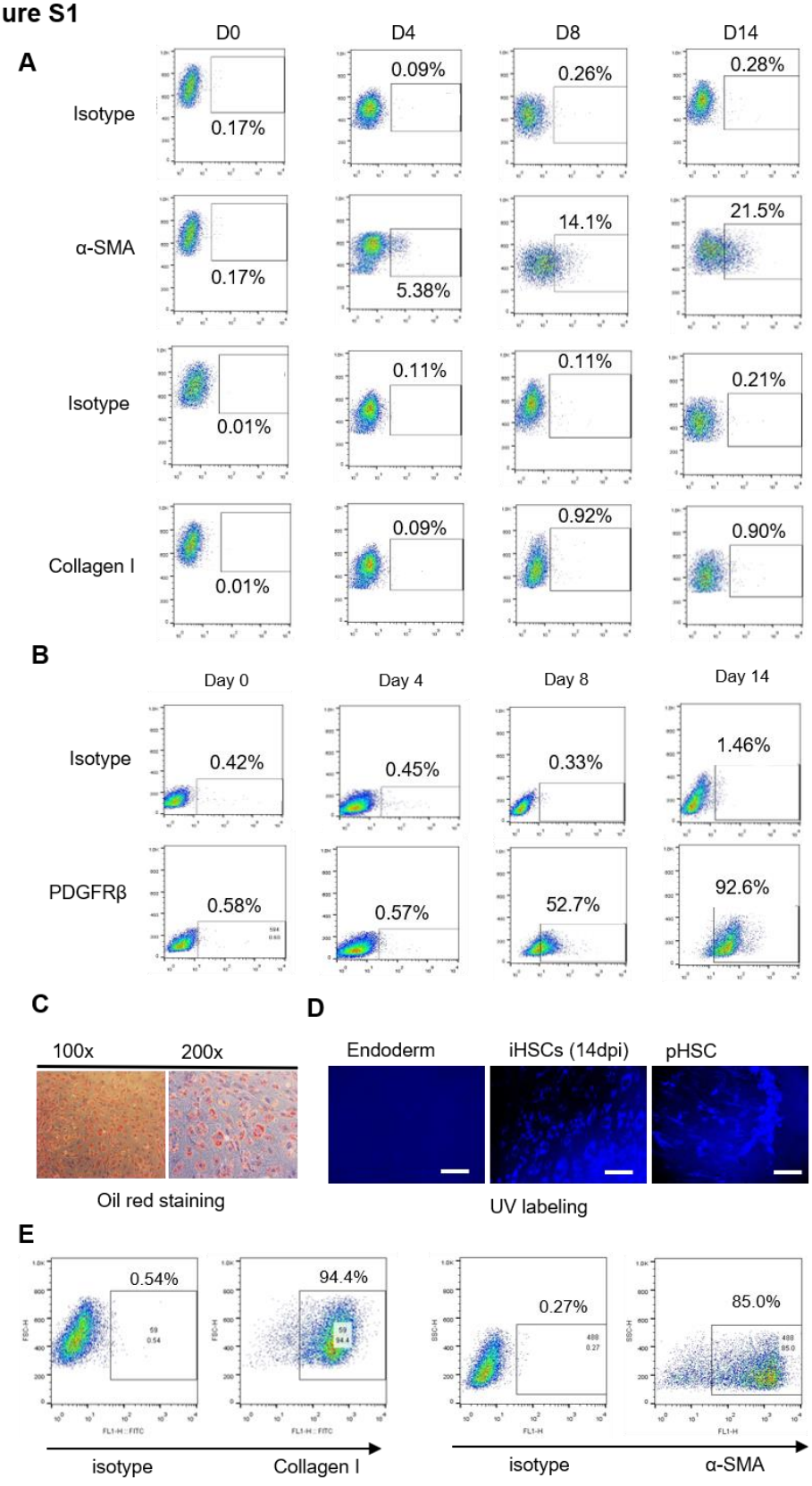

Figure S1. Characterization of endoderm derived iHSCs from hESCs (H9).

Related to Figure 1. (A) Representative flow cytometry plot of α-SMA and collagen I at day 0, 4, 8 and 14 differentiation from hESCs to iHSCs. Positive gates were defined based on the isotype control. (B) Flow cytometry analysis of PDGFRβ at day 0, 4, 8, 14 during the iHSCs differentiation. (C) Representative images of oil red staining analysis of the iHSCs. (D) UV beaching of endoderm, iHSC and pHSC under microscope. Scale bars, 100 μm. (E) Flow cytometry analysis of α-SMA and collagen I in iHSCs during the activation by TGFβ. Positive gates were defined based on the isotype control.

Figure S2

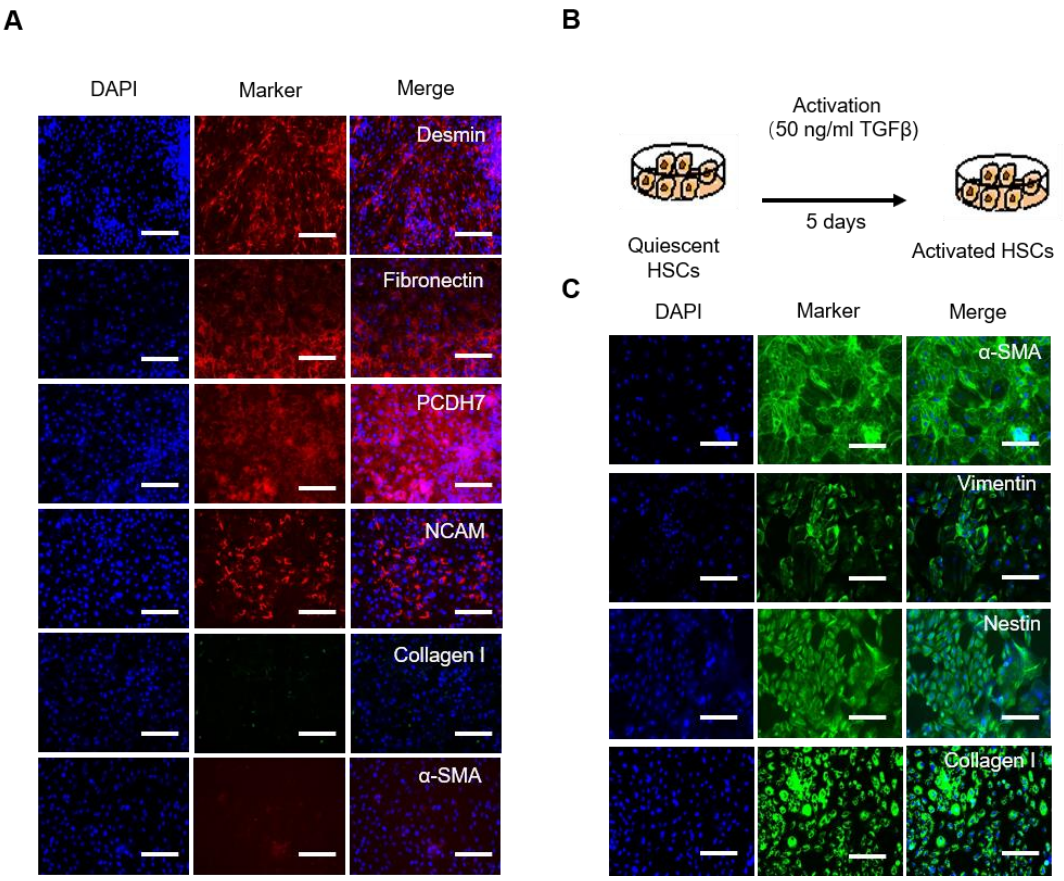
A
DAPI
Marker
Merge
Desmin
Fibronectin
PCDH7
NCAM
Collagen I
α-SMA
B
Activation
(50 ng/ml TGFβ)
5 days
Quiescent
HSCs
Activated HSCs
C
DAPI
Marker
Merge
α-SMA
Vimentin
Nestin
Collagen I

Figure S2. Characterization of iHSCs differentiated from hESCs (H1). Related to Figure 4. (A) Representative images of endoderm derived iHSCs markers expression. Scale bars, 100 μm. (B) Schematic representation of the activation of the iHSCs by TGFβ (50 ng/ml). (C) Representative images of activated iHSCs markers expression. Scale bars, 100 μm.

Figure S3

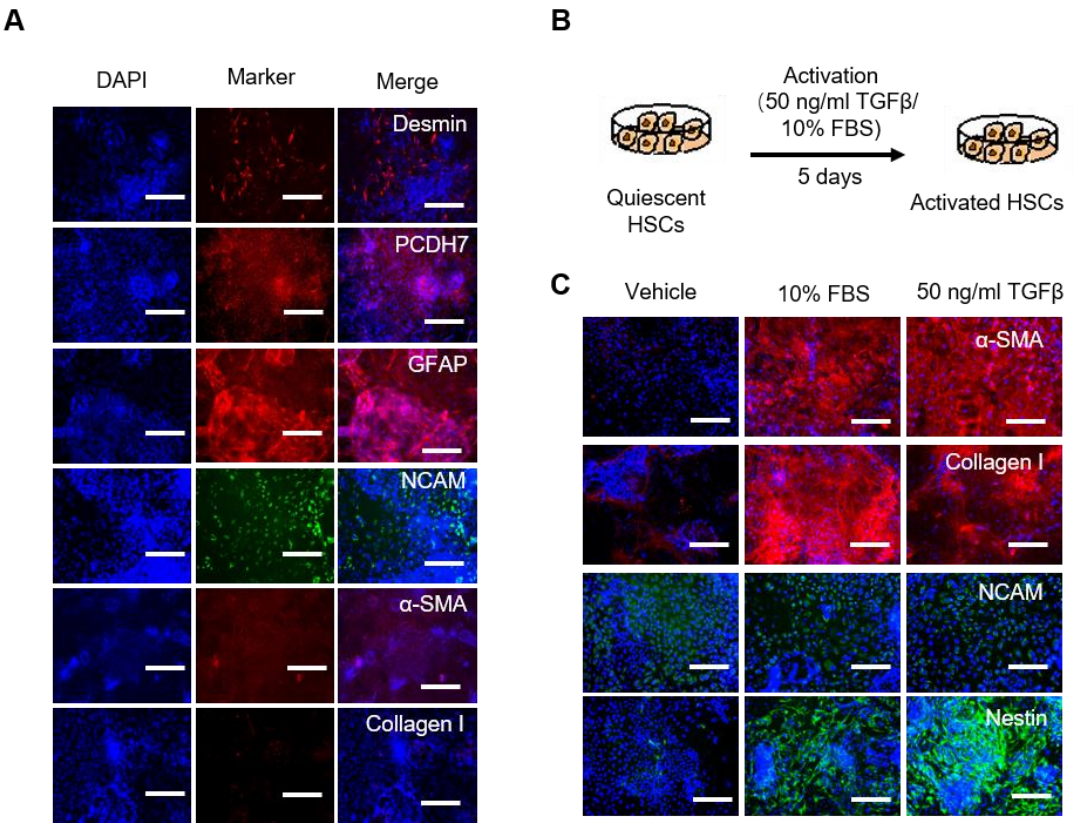
A
DAPI
Marker
Merge
Desmin
PCDH7
GFAP
NCAM
α-SMA
Collagen I
B
Activation
(50 ng/ml TGFβ/
10% FBS)
5 days
Quiescent
HSCs
Activated HSCs
C
Vehicle
10% FBS
50 ng/ml TGFβ
α-SMA
Collagen I
NCAM
Nestin

Figure S3. Characterization of iHSCs differentiated from iPSCs. Related to Figure 4. (A) Representative images of endoderm derived iHSCs markers expression. Scale bars, 100 μm. (B) Schematic representation of the activation of the iHSCs by TGFβ (50 ng/ml) and 10% FBS. (C) Representative images of activated iHSCs markers expression. Scale bars, 100 μm.

Figure S4

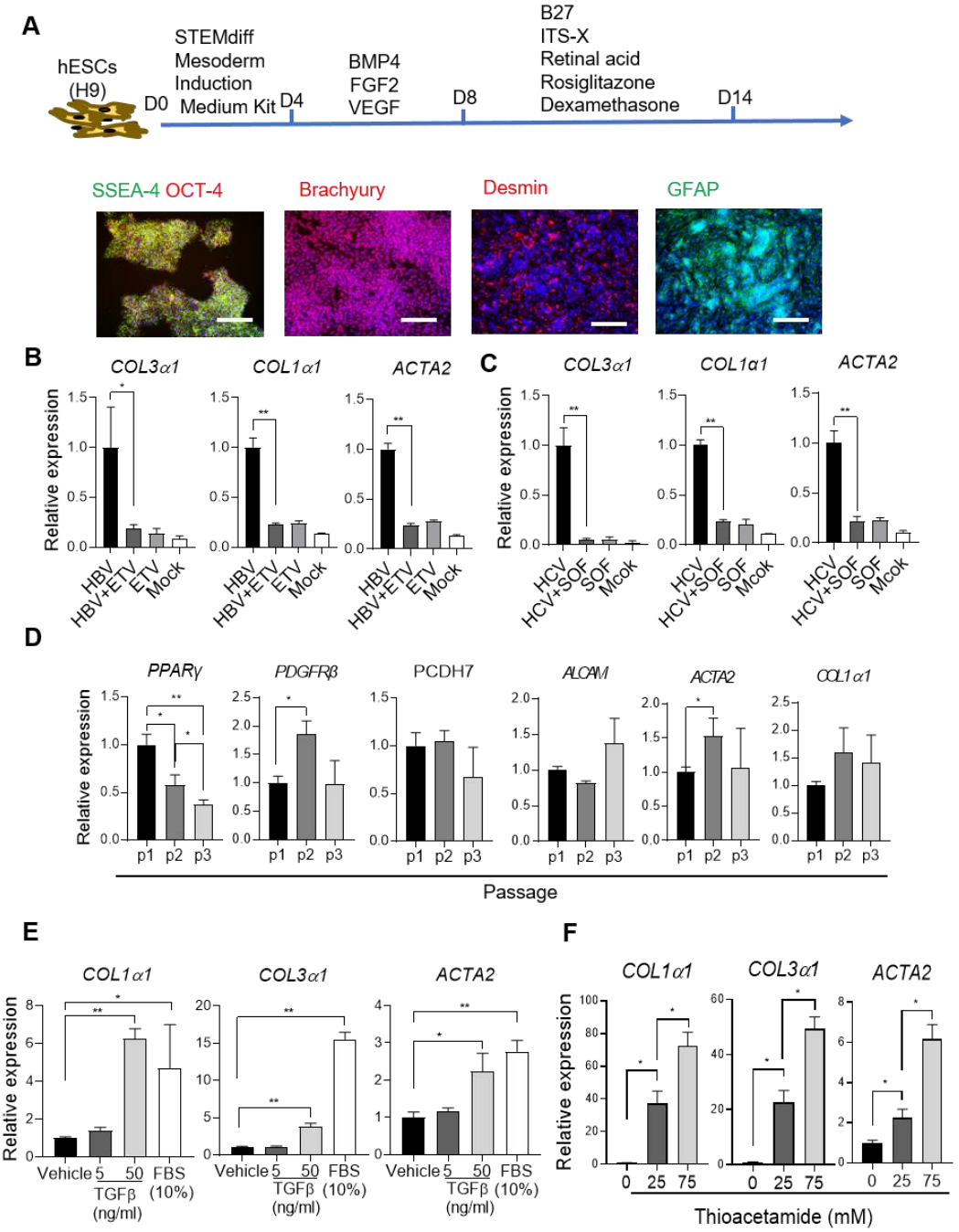
A
hESCs
(H9)
D0
STEMdiff
Mesoderm
Induction
Medium Kit
D4
BMP4
FGF2
VEGF
D8
B27
ITS-X
Retinal acid
Rosiglitazone
Dexamethasone
D14
SSEA-4 OCT-4
Brachyury
Desmin
GFAP
B
COL3α1
COL1α1
ACTA2
Relative expression
HBV
HBV+ETV
ETV
Mock
C
HCV
HCV+SOF
SOF
Mcok
D
PPARγ
PDGFRβ
PCDH7
ALCAM
ACTA2
COL1α1
p1
p2
p3
Passage
E
Vehicle
5
50
FBS
TGFβ (ng/ml)
(10%)
F
Thioacetamide (mM)
0
25
75

Figure S4. Characterization of mesoderm derived iHSCs from hESCs (H9). Related to Figure 7. (A) Representative images of hESCs, mesoderm and iHSCs related markers during the different stage of iHSCs differentiation according to the protocol shown above. Scale bars, 100 μm. (B) RT-qPCR analysis of *COL3α1*, *COL1α1* and *ACTA2* expression in the co-culture of iHSCs and HBV (500 geq/cell) infected HepG2-NTCP with or without entecavir (ETV) (500 nM) treatment for 7 days. (C) RT-qPCR analysis of *COL3α1*, *COL1α1* and *ACTA2* expression in the co-culture of iHSCs and HCV (MOI: 10) infected Huh7.5 cells with or without sofosbuvir (700 nM) for 3 days. (D) RT-qPCR analysis of gene expression in iHSCs at different passages. (E) RT-qPCR analysis of *COL1α1*, *COL3α1* and *ACTA2* expression of the second passaged iHSCs by the treatment of TGFβ and fetal bovine serum (FBS). (F) RT-qPCR analysis of *COL1α1*, *COL3α1* and *ACTA2* expression of the second passaged iHSCs by the treatment of different concentrations of thioacetamide. RT-qPCR data shown as the means±SEM from 3 independent experiments, n=3 in each group. Student's t test was used. *p<0.05.

Figure S5

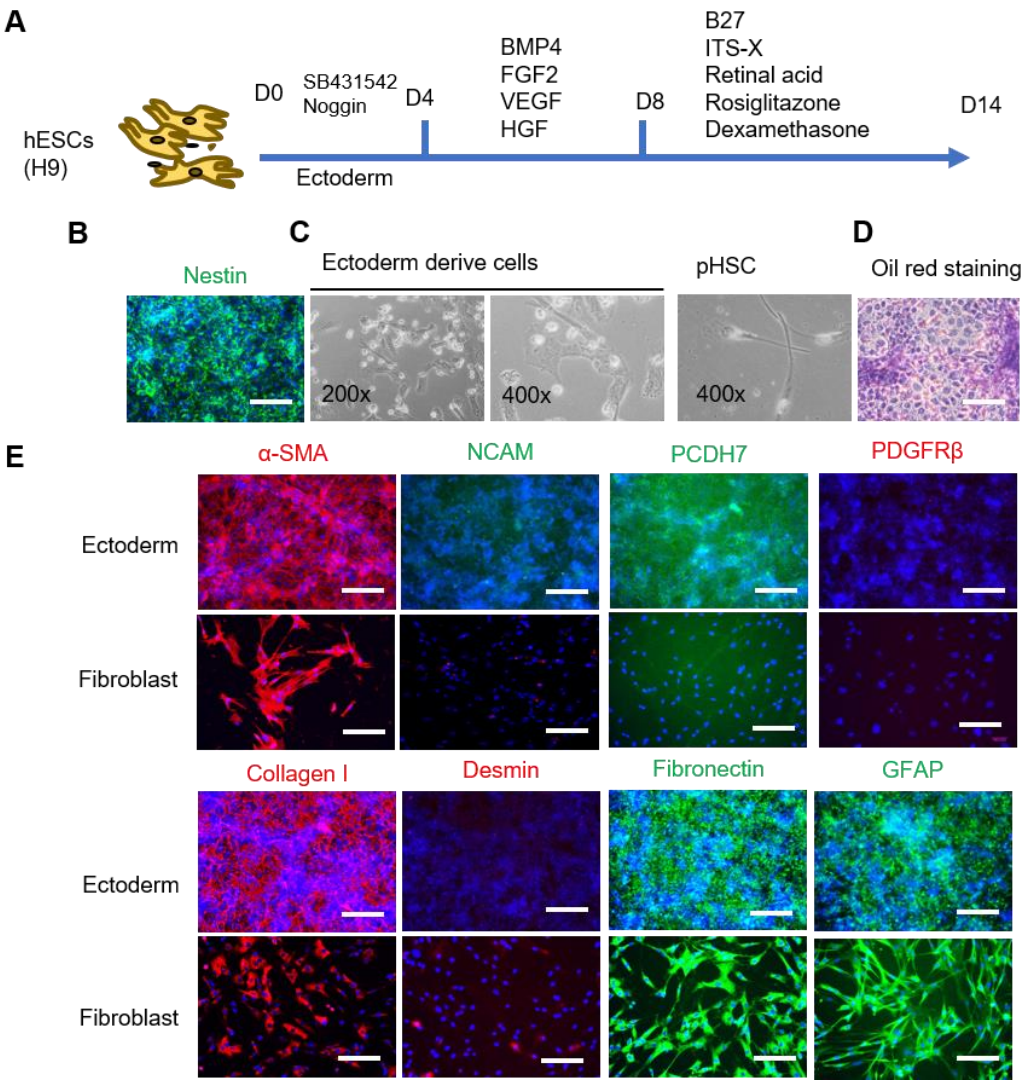
A
hESCs
(H9)
D0
SB431542
Noggin
D4
Ectoderm
BMP4
FGF2
VEGF
HGF
D8
B27
ITS-X
Retinal acid
Rosiglitazone
Dexamethasone
D14
B
Nestin
C
Ectoderm derive cells
200x
400x
pHSC
400x
D
Oil red staining
E
α-SMA
NCAM
PCDH7
PDGFRβ
Ectoderm
Fibroblast
Collagen I
Desmin
Fibronectin
GFAP
Ectoderm
Fibroblast

Figure S5. Characterization of ectoderm derived differentiation by the established differentiation protocol. Related to Figure 7. (A) Schematic representation of the differentiation process from day 0 to day 14. (B) Representative image of nestin expresion in ectoderm. Scale bars, 100 μm. (C) Representative images of cell morphology on day 14 differentiation. (D) Oil red staining analysis of lipid droplet in ectoderm derived cells. (E) Representative images of ectoderm derived cells and fibroblast cells. Scale bars, 100 μm.

Supplementary Tables

Table S1 Top downregulated genes in iHSCs compared to other cells. (See the excel file)

Table S2 Antibodies used for immunofluorescence assay and flow cytometry.

Protein	Supplier	Dilution
α-SMA	Abcam	1/500
ALCAM	Abcam	1/500
β-Actin	Cell Signaling	1/500
Collagen I	Abcam	1/500
Desmin	Abcam	1/500
Fibronectin	Sigma	1/500
NCAM	Sigma	1/500
NGF	Santa Cruz	1/500
PDCH7	Abcam	1/500
PDGFRβ	Abcam (Cambridge. UK)	1/500
Vimentin	Sigma	1/500
SSEA-4	Stem cell	1/500
Nestin	R&D Systems	1/500
Sox17	R&D Systems	1/500
Brachyury	CST	1/500
GFAP	R&D Systems	1/500
AFP	Sigma	1/500

Table S3. List of primers.

Gene	Forward (5'→3')	Reverse (5'→3')
GAPDH	AGCCACATCGCTCAGACAC	GCCCAATACGACCAAATCC
RPS11	GCCGAGACTATCTGCACTAC	ATGTCCAGCCTCAGAACTTC
COL1α1	GACACAGAGGTTTCAGTGG	CACCCTTAGCACCAACAG
COL3α1	GGAGCTGGCTACTTCTCGC	GGGAACATCCTCCTTCAACAG
ALB	TGGCACAATGAAGTGGGTAA	CTGAGCAAAGGCAATCAACA
PDGFRα	AACCCTGCTGATGAAAGCAC	TCCTTTCTAGCATGGGGACA
Desmin	AGGAACAGCAGGTCCAGGTA	AGAGCATCAATCTCGCAGGT
GFAP	GGATGGAGAGGTCATTAAGGA	GGTGAGTTTCTTGTTAGTTGGA
PDGFRβ	CCCTTATCATCCTCATCATGC	CCTTCCATCGGATCTCGTAA
Oct-4	GATGGCGTACTGTGGGCCC	TGGGACTCCTCCGGGTTTTG
ALCAM	ACCTCAGAATCTCATGTTTGG	GTTTAGATGGTTGCTTGAACAC
ACTA2	CCAGAGCCATTGTCACACAC	CAGCCAAGCACTGTCAGG
NCAM	AGGAGACAGAAACGAAGCCA	GGTGTTGGAAATGCTCTGGT
FOXA2	ATTGCTGGTCGTTTGTTGTG	TACGTGTTCATGCCGTTCAT
SOX17	CGCACGGAATTTGAACAGTA	GGATCAGGGACCTGTCACAC
hSTAP	TGCCAGTGACTTCCCACCT	TAGATGAGGCCACGCAGC
AFP	AGA CTG AAA ACC CTC TTG AAT GC	GTC CTC ACT GAG TTG GCA ACA
PCDH7	GGATCGGGTGAGGTGACTTTC	GTTCTCGTCGAAGATCATCTGAC
THY-1	AAGGACGAGGGCACCTACAC	GAGGTGTTCTGAGCCAGCAG
PPARγ	GAGGAGAGTTACTTGGTCGT	CAACAGACAAATCACCATTCG

Supplementary Experimental Procedures

Immunofluorescence staining

The immunofluorescence staining for related markers expression was performed as previously described (Coll et al., 2018). Briefly, cells were fixed in 4% para-formaldehyde in phosphate-buffered saline (PBS) at room temperature for 10 min and permeabilized with 0.1% Triton X-100 in PBS. Then, the cells were blocked with blocking buffer [PBS containing 10% goat serum, 1% bovine serum albumin (BSA)] at room temperature for 2 h. Cells were incubated overnight at 4 ℃ with primary antibody diluted with blocking buffer. Secondary antibodies (1:1000 dilution) were incubated in dark at room temperature for 1 h. Nuclei were stained with 4',6-diamidino-2-phenylindole (DAPI) diluted in PBS at room temperature for 20 min. Antibodies and dilutions used are listed in Table S2.

Quantitative real-time RT-PCR

Total RNA was obtained by using the RNAeasy Mini Kit (QIAGEN) followed by reverse transcription with Superscript III First-Strand Synthesis System. Gene expression was determined by quantitative real-time PCR on ABI 7500 cycler using Powerup SYBR master mix (Life technologies). The gene expression was normalized to RPS11 and calculated with the comparative Ct method ($2^{-\triangle\triangle Ct}$). Primers are listed in Table S3.

Flow cytometry

Differentiated cells were dissociated into a single-cell suspension and stained with antibodies for COT4, SSEA4, Brachyury, PDGFRβ, PDGFRα, Collagen I and α-SMA. Stained cells were analyzed with FACSCanto II cytomerter and FlowJo VX software. FACS plot showing populations were usually 10,000 and the positive gates were defined based on the isotype control.

Oil red staining

The differentiated cells at day 14 were analyzed for the vitamin A uptake by oil red staining. Cells were washed by DPBS for three times and fixed with 4% para-formaldehyde in PBS at room temperature for 10 min followed by 60% isopropanol washing. Then, cells were incubated with Oil Red (Sigma) working solution (6:4 Oil Red: ddH2O) for 30 min at room temperature. Finally, cells were counterstained with Gill's hematoxylin and washed with PBS. The images were performed by a fluorescence microscope (ECHO laboratories, USA)

Vitamin A storage assay

The vitamin A storage assay was performed as previously described. Briefly, the differentiated cells at day 14 were measured by the auto-fluorescence after UV light excitation and flow cytometry.

Genome wide transcriptome analysis of iHSCs

RNA-seq was performed at Novogene Co. Ltd. Total RNA was isolated from endoderm derived iHSCs (iHSC-end, n=3 independent differentiations), mesoderm derived iHSCs (iHSCs-M_2, n=3 independent differentiations), fibroblast (n=3 independent fibroblast cells), purchased primary HSCs (purHSC, n=3 independent donors cells bought from Lonza) and freshly pHSCs isolated from liver transplantation patients (n=3 different liver donors). Total RNA was isolated by using the RNeasyMini Kit (QIGEN). RNA sequencing libraries were prepared by using the NEBNext UltraTM RNA library Prep kit for Illumina (NEB) following the manufacturer's instructions. The randomly primed 150-bp paired-end libraries were sequenced on Illumina Hiseq 4000 platform. Raw data for human quiescent HSC (Liu et al., 2020) (qHSCs, GSE141100), hepatocyte (Jacquemin et al., 2013) (hep, GSE43984) and cultured hepatocytes (Koui et al., 2017) (cul_hep, GSE43984) and the iPSC-derived qHSC like cells (Koui et al., 2021) (TkDN4_M_qHSCs and FF-1_qHSCs, GSE155017) were extracted from GEO. The reads were aligned to the human genome (hg38) using STAR v2.7.9a (Dobin et al., 2013) and gene expression levels were estimated using featureCounts (Liao Y et al, 2014). DESeq2 (Love et al., 2014) was used to perform differential gene expression analysis. The HSC gene set signature previously described (Coll et al., 2018) was used to perform a gene set enrichment analysis (GSEA). DAVID bioinformatics Resources 6.8 R package clusterProfiler was used to perform gene ontology (GO) and KEGG pathway analysis (Wu et al., 2021). Principal component analysis (PCA) was generated with R PCA function using scaled gene expression. Heatmaps were generated by the pheatmap package.

Transwell co-culture of HepaRG with iHSCs or pHSCs

HepaRG cells were cultured in the HepaRG culture medium (Biopredic). Differentiated HepaRG cells (60,000 cells/well) were seeded in the insert of the transwell cultured in the Serum-free HepaRG medium. At the same time, the endoderm and mesoderm derived iHSCs (80,000 cells/well) were cultured in the plates. Then, the inserts were transferred in the iHSCs or pHSCs wells to form HepaRG co-cultured with iHSCs. As a positive control, iHSCs were replaced by primary human HSCs.

Exposure of iHSCs to acetaminophen and thioacetamide

Differentiated iHSCs cells were seeded at 80,000 cells per well in the Matrigel coated 24-well plate. Acetaminophen and thioacetamide at the concentration of 0, 25 and 75 mM were added to treat the cells for 48 h. The cells were harvested to analyze the activation of iHSCs by hepatotoxin exposure. Cell viability assay was performed by CellTiter-Blue assay as manufacturer's instructions.

Exposure of co-cultured iHSCs/pHSCs and HepaRG to acetaminophen

Differentiated HepaRG cells (60,000 cells/well) were seeded in the insert of the transwell cultured in the serum-free HepaRG medium. The bottom of the transwell plate was seeded with the iHSCs or pHSCs (80,000 cells/well). The cells were put in a well for co-culture. The cells were exposed to the 0, 25 and 75 mM of acetaminophen for 48 h. RT-qPCR assay was performed to analyze the mRNA levels of HSCs activated

markers. Cell viability assay was performed by CellTiter-Blue assay as manufacturer's instructions (Coll et al., 2018).

Exposure of iHSCs to HBV infected HepG2-NTCP cells

HepG2-NTCP cells (60,000 cells/well) were seeded in the insert of the transwell plate and infected with HBV (500 geq/cell) for 24 h. The next day, the cells were washed with PBS and replenish with fresh serum-free differentiation medium and co-cultured with iHSCs (80,000 cells/well) respectively for seven days. 500 nM of entecavir (ETV) was used as control for inhibition of HBV replication (Michailidis et al., 2017).

Exposure of iHSCs to HCV infected Huh7.5 cells

Huh7.5 cells (60,000 cells/well) were seeded in the insert of the transwell plate and infected with HCV (JFH1, MOI:10) for 24 h. The next day, the cells were washed with PBS and replenish with fresh serum-free differentiation medium and co-cultured with iHSCs (80,000 cells/well) respectively for three days. The 700 nM of sofosbuvir (SOF) was used as control for inhibition of HCV replication (PascalMutz et al., 2018).

***In vitro* activation of iHSCs**

Differentiated cells at day 14, iHSCs were seed with 60 thousand per well in the 24-well plate and activated by incubating with Transforming Growth factor β (TGFβ) (5 ng/ml or 50 ng/ml) or FBS (10%) for different days as designed. RT-qPCR was used to evaluated stellate cells activation related gene expression after different days of

incubation.

In vitro wound-healing assay

After performed a scratch, the differentiated cells and primary HSCs were stimulated with 25 ng/ml PDGF-BB (Sigma) and 10% FBS for 24h. Images were captured with a fluorescence microscope (ECHO laboratories, USA). The wound closure distances were measured using ImageJ software.

Measurement of secreted collagen I

The secreted collagen I was detected by the chemiluminescence immunoassay (CLIA) kit according to the manufacturer's instructions (Ding Sheng Xing Ye Co.) detected by manufacturer-provided luminometer.

References

Coll, M., Perea, L., Boon, R., Leite, S.B., Vallverdu, J., Mannaerts, I., Smout, A., El Taghdouini, A., Blaya, D., Rodrigo-Torres, D.*, et al.* (2018). Generation of hepatic stellate cells from human pluripotent stem cells enables in vitro modeling of liver fibrosis. Cell Stem Cell *23*, 101-113 e107.

Jacquemin, M.G., Covens, K., Jazouli, N., Sokal, E., Peerlinck, K., and Shahani, T. (2013). Human liver sinusoidal endothelial cells but not hepatocytes contain FVIII. J Thromb Haemost *11*, 323-323.

Koui, Y., Himeno, M., Mori, Y., Nakano, Y., Saijou, E., Tanimizu, N., Kamiya, Y., Anzai, H., Maeda, N., Wang, L.*, et al.* (2021). Development of human iPSC-derived quiescent hepatic stellate cell-like cells for drug discovery and in vitro disease modeling. Stem Cell Reports *16*, 3050-3063.

Koui, Y., Kido, T., Ito, T., Oyama, H., Chen, S.W., Katou, Y., Shirahige, K., and Miyajima, A. (2017). An in vitro human liver model by iPSC-derived parenchymal and non-parenchymal cells. Stem Cell Reports *9*, 490-498.

Liu, X., Rosenthal, S.B., Meshgin, N., Baglieri, J., Musallam, S.G., Diggle, K., Lam, K., Wu, R., Pan, S.Q., Chen, Y.*, et al.* (2020). Primary alcohol-activated human and mouse hepatic stellate cells share similarities in gene-expression profiles. Hepatol Commun *4*, 606-626.

Michailidis, E., Pabon, J., Xiang, K.H., Park, P., Ramanan, V., Hoffmann, H.H.,

Schneider, W.M., Bhatia, S.N., de Jong, Y.P., Shlomai, A.*, et al.* (2017). A robust cell culture system supporting the complete life cycle of hepatitis B virus. Sci Rep *7*, 16616.

PascalMutz, PhilippeMetz, FlorianA.Lempp, SilkeBender, BingqianQu, KatrinSchöneweis, StefanSeitz1ThomasTu, AgneseRestuccia, JamieFrankish, ChristopherDächert*, et al.* (2018). HBV bypasses the innate immune response and does not protect HCV from antiviral activity of interferon. Gastroenterology *154*, 1791-1804.

Wu, T., Hu, E., Xu, S., Chen, M., Guo, P., Dai, Z., Feng, T., Zhou, L., Tang, W., Zhan, L.*, et al.* (2021). clusterProfiler 4.0: A universal enrichment tool for interpreting omics data. Innovation *2*, 100141.